CLNS-378
November 1977
DESY 77/71

Hadron Production by Electrons in the Deep-Inelastic Region[$†]

by

I. Cohen, R. Erickson, F. Messing[+], E. Nordberg, R. Siemann, J. Smith-Kintner, and P. Stein
Cornell University, Ithaca, N.Y.,

and

G. Drews, W. Gebert, P. Joos, A. Ladage, H.J. Nagel[x], and P. Söding
Deutsches Elektronen-Synchrotron DESY and University of Hamburg

and

A. Sadoff
Ithaca College, Ithaca, N.Y.

Abstract

An experiment was made to study the complete hadronic final states in deep-inelastic electron proton interactions in the kinematic range $0.5 < Q^2 < 6$ GeV^2 with $\langle Q^2 \rangle = 2.2$ GeV^2 and $\sqrt{s} = W$ up to 4.2 GeV. Results are reported on multiplicities, longitudinal distributions and fragmentation functions, behavior of the transverse momentum, inclusive K^o, Λ and ρ^o production, and charge retention.

† Contribution to the 1977 International Symposium on Lepton and Photon Interactions at High Energies, Hamburg, August 25-31, 1977

$ Work supported in part by the National Science Foundation and the Bundesministerium für Forschung und Technologie.

+ Now at Carnegie-Mellon University, Pittsburgh, PA

x Now at Beiersdorf AG, Hamburg 20

1. Experimental Method

In this paper we present results on the final hadronic states produced in deep-inelastic electron-proton scattering. The experiment was performed at the Cornell University electron synchrotron in an 11.5 GeV beam. The target was surrounded by a streamer chamber, in which the momenta of the scattered electron and all outgoing charged hadrons were measured. The chamber had a sensitive volume of 100 x 60 x 45 cm^3 and was placed in a homogeneous magnetic field of 1.65 T.

The beam was incident on a 9 cm long 1.5 cm diameter liquid hydrogen target inside the streamer chamber. To detect and identify the scattered electron, arrays of scintillation and shower counters were placed behind the chamber on both sides of the beam (Fig.1a,b).The streamer chamber was triggered when a scattered electron was detected. Proportional chambers in the trigger arms were used to improve the momentum and angular resolution of the scattered electron and of the hadrons in the forward direction.

The total data sample consists of about 130 000 ep-scattering events in the kinematic region $0.5 < Q^2 < 6$ GeV^2 and W up to 4.2 GeV. The pictures from the streamer chamber were measured on a flying-spot digitizer. The geometrical reconstruction and the kinematic fits were made using the CERN bubble-chamber analysis programs THRESH and GRIND.

All results presented in this paper are preliminary and are based on 20 % of the complete data (except for the results on strange particle production which are based on 75 % of the data).

2. Charged Multiplicities

We have determined the mean charged hadronic multiplicity, $\langle n_{ch} \rangle$, using a subsample of our data. In this subsample (10% of our total data) the film was scanned twice, and all events failing the reconstruction programs were remeasured. For approximately 85 % of the completely reconstructed events, the proper total hadronic charge is observed. The remainder of the sample was corrected for the missing charge. Radiation corrections were made for each topological cross-section individually. Finally, small corrections are made for the variation of the acceptance in Q^2 and W.

In Fig. 2 is shown the variation of $\langle n_{ch} \rangle$ with Q^2 for various ranges of W. Our data are consistent with the previous observation that $\langle n_{ch} \rangle$ does not vary significantly with Q^2 in the deep inelastic region. Photoproduction points are shown for comparison.

Fig. 3 shows the variation of $\langle n_{ch} \rangle$ with W^2 for all events with $Q^2 > 1$ GeV^2. Our data are in agreement with previous leptonic production data for $W^2 < 10$ GeV^2. For $W^2 > 10$ GeV^2, our data show a continual rise which is somewhat in disagreement with a previous measurement of $\langle n_{ch} \rangle$ in $\mu^+ p \to \mu^+ X$. On the other hand, our data agree with $\langle n_{ch} \rangle$ as measured in e^+e^-, pp, and πp reactions, as well as with a previous measurement of $e^- p \to e^- X$.[1]

We have also calculated the mean charged multiplicity $\langle n_{ch} \rangle_z$ as a function of $z = p_h/\nu$. p_h is the momentum of any hadron in the final state, and $\nu = E_{inc} - E_{sc}$ is the energy loss of the electron in the laboratory. It has been suggested that such a measurement can be used as a consistency check of a color gluon model of lepton hadron inelastic scattering.[2] In this model, it is expected that $\langle n_{ch}(W^2) \rangle_z = 1 + \langle n_{ch}((1-z)W^2) \rangle$. The curve in Fig. 4 shows this prediction, where $\langle n_{ch}((1-z)W^2) \rangle$ is the mean charged multiplicity at a center of mass energy squared of $(1-z)W^2$, and is taken from our data. The agreement is excellent.

3. Quark Fragmentation

In the quark parton model, the production of hadrons by virtual photons can be viewed as a two stage process.[3] In the first stage, the virtual photon's momentum is absorbed by a single quasi-free quark. Assuming that the internal motion of the quarks within the proton can be ignored, the struck quark separates itself from the remainder of the proton by virtue of its sudden change in momentum. In the second stage, the struck quark converts into real hadrons referred to as the current fragments. The current fragments are expected to have limited transverse momentum with respect to the quark's direction, and also to retain the bulk of the virtual photon's momentum. This model predicts that the production distributions $N^h(z,\vec{p}_\perp; R)$ for the forward hadrons can be written as products of the probability $D_q^h(z,\vec{p}_\perp)$ that a quark q will fragment into a hadron with relative three-momentum $z = p_h/\nu$ and transverse momentum $\vec{p}_\perp$, times the probability $f_q(R)$ that a quark q was struck in the kinematic region R, i.e.

$$N^h(z,\vec{p}_\perp;R) = \sum_q f_q(R)\, D_q^h(z,\vec{p}_\perp) \qquad (1)$$

With the normalization $\int_R \sum_q f_q(R) = 1$ the function $N^h(z,\vec{p}_\perp;R)$ gives the number of hadrons of type h per bin of $dzd^2\vec{p}_\perp$ produced per event in the kinematic region R.

These ideas are expected to apply in the deep-inelastic region where Q^2 and W^2 are much greater than the square of the proton mass. However, measurements have shown that the parton model describes the total cross section over a more extended region down to $Q^2 = 1$ GeV^2 and $W = 1.8$ GeV.[4] The question then arises as to the validity of more detailed parton ideas in this extended region.

To test these ideas, we integrate the sum of positive and negative hadrons, $N^{h+} + N^{h-}$, over transverse momentum and azimuthal angle. Using the symmetry properties of the D functions under isospin and charge conjugation, equation (1) leads to the simple prediction for pions that

$$N^{\pi^+}(z;R) + N^{\pi^-}(z;R) = D_u^{\pi^+}(z) + D_u^{\pi^-}(z) = D_d^{\pi^-}(z) + D_d^{\pi^+}(z) \qquad (2)$$

where u and d refer to up and down quarks respectively, and we have neglected strange and charmed quarks; i.e., within this model, the production of charged pions is independent of the kinematic region R of the virtual photon-proton system, as long as this region is not dominated by the $q\bar{q}$ sea.

In Fig. 5, we show $N^{h^+} + N^{h^-}$ for six kinematic regions R defined by cuts on Q^2 and $x' = Q^2/(Q^2 + W^2)$. Even in the current fragmentation region, i.e. at large z, this sum depends on x'. When only events at high W are taken, this dependence is no longer statistically significant (see Fig. 6).

An alternative way of viewing the data is to plot the multiplicity at high z,

$$N^h(W^2) = \int_{0.4}^{1} (N^{h+}(z,W^2) + N^{h-}(z,W^2))dz \ .$$

Fig. 7 shows that $N^h(W^2)$ falls with increasing W^2 at both high and low Q^2.

We have looked at measurements of the proton spectrum to determine whether this W^2 dependence is due to proton contamination. Proton contamination is a worry because essentially all protons produced in the forward hemisphere ($x_F > 0$) in the center-of-mass appear at $z \gtrsim .4$. An estimate of the proton contribution to our data at high z, based on the measurements of Bebek et al.[5], is also shown in Fig. 7. After subtraction of this proton estimate the behavior of $N^h(W^2)$ from our data is not inconsistent with being independent of W for $W^2 > 7$ GeV^2, as indicated by the dashed line in Fig. 7.

It is also consistent with the forward multiplicity measured at very high W at Fermilab[6].

We conclude that a major part of the W^2 dependence in Fig 7 is due to proton contamination and that at high W and large z proton contamination is not a serious problem with our data.

Bebek et al[5] have shown that at a fixed W, the forward proton distribution does not depend on Q^2 (and hence on x' since W is fixed). We can therefore test the parton model without serious bias due to protons by considering

$$N^h(x') = \int_{0.4}^{1} (N^{h+}(z,x') + N^{h-}(z,x'))dz$$

for narrow W regions. The results are shown in Fig 8. Within errors, no x' dependence at fixed W is discernable. This result lends support to the ideas of the quark parton model down to W^2 of 6 GeV^2.

Another prediction of the parton model as summarized in equation (1) is that the difference between the number of positive and negative pions is[7]

$$N^{\pi^+}(z,R) - N^{\pi^-}(z,R) = \xi(R)(D_u^{\pi^+}(z) - D_u^{\pi^-}(z)) \qquad (3)$$

The factor $\xi(R)$ relates the probabilities that a u quark or a d quark was struck in the kinematic region R. Eq(3) predicts that $N^{\pi^+} - N^{\pi^-}$ should have a z dependence which is separable from the kinematic variables of the electron. In contrast to equation (2), however, equation (3) has an x-dependent normalization factor $\xi(R)$. In Fig 9, we compare the z dependencies of this difference for various x intervals. An arbitrary normalization factor has been introduced for each x interval. A W^2 cut of 9 GeV^2 was used to minimize proton contamination; a higher W^2 cut would have been desirable, but our present data sample does not have sufficient statistical significance to perform this test with a higher cut. No significant variation with x is seen, confirming the factorization in x and z predicted by eq.(3).

In Fig. 10, we compare our hadron distribution with those measured in e^+e^- and other lepton scattering experiments including data on π^o production[8-10]. The probability that any quark will fragment into a π^o is expected to be the average of the probabilities for it to fragment into a π^+ or a π^-,

$$D_q^{\pi^o}(z) = (D_q^{\pi^+}(z) + D_q^{\pi^-}(z))/2.$$

Thus, we expect

$$N^{\pi^+}(z) + N^{\pi^-}(z) = 2N^{\pi^o}(z) .$$

We would also expect to find the same hadron distribution in e^+e^- neglecting the small $s\bar{s}$ contribution. In e^+e^- annihilation reactions there are two quarks fragmenting, and therefore

$$(N^{h^+}(z) + N^{h^-}(z))_{eP} \simeq 1/2\ (N^{h^+}(z) + N^{h^-}(z))_{e^+e^-}$$

The results of our own data plotted in Fig 10 are for $Q^2 > 1$ GeV^2 and $W^2 > 12$ GeV^2 in order to minimize proton contamination. We have examined the contribution of elastic ρ^o production in this range and find it smaller than the statistical errors.

The band shown in Fig 10 is a fit by Field and Feynman to previous data from e^+e^- and lepton scattering experiments[11]. In addition to our own data, we have plotted other data submitted to this conference from the reactions $e^+e^- \to h^\pm X$ [9,10] and $e^-p \to e^-\pi^o X$. [8] In the high-z region, our data agree better with the compilation of Field and Feynman than with the new storage ring results. At the lower z values, we agree with the new e^+e^- results; however, in this range we may well have proton contamination from target fragmentation.

Finally, we can determine the fragmentation functions $D_u^{\pi^+}$ and $D_u^{\pi^-}$ from the sum and difference of positive and negative hadrons (Eq (2) and (3)). The small kaon contribution has been neglected. We use only our data at $x = Q^2/2m\nu > 0.1$ in order to exclude the region of strong $q\bar{q}$ contributions. Single arm electron scattering data were used to determine $\xi(R)$, since $\xi(R)$ is related to the ratio of proton and neutron cross sections. We found $\langle\xi\rangle = 0.70$ to be the average over our kinematic range.

In Fig 11, we have plotted the results for $zD_u^{\pi^+}(z)$ and $zD_u^{\pi^-}(z)$ from our data. The curves show estimates of these functions by Field and Feynman[11]. Our determination of these functions will of course be rendered incorrect by any residual proton contamination in $N^{h+}(z)$. We therefore estimated this contamination in our kinematic region by extrapolating the inclusive proton data of Bebek et al[5] to higher W. After subtraction of this estimate for the protons from $N^{h+}(z)$, the $zD_u^{\pi^-}(z)$ now obtained has hardly changed, while the result for $zD_u^{\pi^+}(z)$ for $z < 0.4$ is considerably smaller than the value obtained without proton subtraction. It is clear that this latter result cannot be taken as quantitatively correct, due to uncertainties in the proton subtraction, but it can serve to illustrate the qualitative behavior of these functions.

4. Transverse Momentum

The transverse momentum $p_\perp$ of the hadrons is defined with respect to the direction of the virtual photon. As an example of the distributions measured, Fig. 12 shows $(1/\sigma_{tot})d\sigma/dp_\perp^2$ for $3 < W < 4.2$ GeV and various ranges of Q^2 between 0.5 and 6 GeV^2 at low and at high z. These distributions show no significant variation with Q^2. On the other hand, they depend strongly on z. In the low-z region, the shape of the distributions can be well fitted by the functional form $Ae^{-Bp_\perp}$, while for the large-z region the dependence is more like $Ae^{-Bp_\perp^2}$. Neither functional form can be used for both regions. The average value of $p_\perp$ is different in the two regions. $\langle p_\perp \rangle$ is 300 MeV in the low-z region and 460 MeV in the large-z region.

In Fig. 13 to 15, the dependence of $\langle p_\perp \rangle$ on various kinematic variables is shown. Fig. 13a and b show the dependencies of $\langle p_\perp \rangle$ on Q^2 and $x = Q^2/2m\nu$, separately for hadrons in two different z ranges, for W between 3 and 4.2 GeV. We observe no variation of $\langle p_\perp \rangle$ with Q^2 and x (which are related because of the limited range of W). Fig. 13c shows a modest increase of $\langle p_\perp \rangle$ with W over the range $1 < W < 4.2$ GeV. The z dependence of $\langle p_\perp \rangle$ in several W regions is shown in Fig. 14. Finally, Fig. 15a shows that the independence of $\langle p_\perp \rangle$ on x (and therefore on Q^2, at fixed W) holds throughout the whole W range covered in this experiment, within our statistical accuracy.

Related observations have been made in other lepton scattering experiments.[12-16,25] Since in most other experiments instead of z the longitudinal variable $x_F = p^*_{h\parallel}/p^*_{h\ max}$ was used, we also show in Fig. 15b the dependence of $\langle p_\perp \rangle$ for negative hadrons as a function of W for various bins in x_F. Within the statistical accuracy no strong dependence on W, in fixed regions of x_F, is seen. This preliminary result is at variance with other reported results.[15] Our values of $\langle p_\perp \rangle$ for all hadrons with $z > 0.3$ are consistent with the νp result of ~450 MeV. $\langle p_\perp \rangle$ is largest in the bin of highest x_F in Fig. 15b, in accordance with the behavior observed in other experiments. Comparing Figs. 13 and 15b one should note that averages of $p_\perp$ taken at constant x_F are smaller than averages at constant z. This is due to the fact that at constant x_F, with increasing $p_\perp$ also z increases such that the hadron distribution function decreases, giving relatively smaller weights to the region of larger $p_\perp$'s.

The value $\langle p_\perp \rangle \simeq 300$ MeV observed for $0 < z < 0.3$ is reminiscent of the average transverse momentum with respect to the jet axis found in e^+e^- annihilation.[17] The larger average $\langle p_\perp \rangle \simeq 460$ MeV that we find for fast hadrons ($z>0.3$) may suggest

that a transverse momentum $p_{q\perp}$ of the quark in the target proton could be contributing to the transverse momentum of the hadron. The leading hadrons from a fragmenting quark will take a larger fraction of $p_{q\perp}$ than the hadrons emitted at small z, which may account for the observed increase of $\langle p_\perp \rangle$ with fractional hadron momentum z. Interpreting our data in this way, a preliminary estimate suggests a value of the average quark transverse momentum $\langle p_{q\perp} \rangle$ on the order of 500 MeV. The effect of the transverse momenta of the quarks bound in nucleons may also have been seen in hadronic reactions at high $p_\perp$ and in lepton pair production[18,26]. The observed x-independence of $\langle p_\perp \rangle$ of the hadrons emitted at high z in our experiment would further argue in favor of a mean quark transverse momentum $\langle p_{q\perp} \rangle$ that is independent of x in the range $0.05 < x < 0.45$.

Finally, in Fig. 16 it is shown that the ratio of positive to negative hadrons increases with the transverse momentum of the hadron.

5. Electroproduction of Neutral Strange Particles

A special scan was made for events with a neutral vertex outside of the target region. The three major sources of these vertices are Λ decay, K^o_S decay, and photon conversion. These latter events are easily eliminated because the electron positron pairs have a small opening angle, and the pair production occurs predominantly in the center electrode of the streamer chamber. Eliminating these photons from the sample, requiring that the neutral particle come from the interaction vertex and assuming proton and pion masses for the positive and negative tracks respectively yields the mass distribution shown in Fig. 17a. Approximately 25 % of the Λ's would also be identified as K^o's under the assumption that the final two particles are pions. However, by Monte Carlo studies of K^o and Λ decays and by looking at the mass distributions for the assumptions of $\bar{p}$ and π^+, we are convinced that events with two possible identifications are most probably Λ's, and we treat them as such. Approximately 3 % of the K^o sample appear as contamination in the Λ sample. A mass distribution for the assumption of $\pi^+\pi^-$ after photons and Λ's have been removed from the sample is shown in Fig. 17b.

Small corrections to the number of K^o's and Λ's are necessary to correct for the efficiency of particle identification. A much more significant correction must be applied to the data to account for portions of the solid angle where a decay could not be observed. Decays in either the target, target vacuum box or beam tube would not be seen. Events were weighted according to the length of path in these regions when plotting the data. The resultant correction for

unobserved decays is approximately a factor of 3. The corrected number of events is consistent with the number expected from a plot of measured lifetimes.

The z distribution for the production of K_S^o is shown in Fig. 18 compared with the spectrum measured at 3.6 GeV by the PLUTO group at DORIS.[19] The comparison is in shape only and not in absolute magnitude, and the agreement is excellent. We expect leading K_S^o's to be fragments of d, $\bar{d}$, s and $\bar{s}$ quarks, and in the colliding beam experiment all of these quarks should contribute to the K_S^o yield. Since $x = Q^2/2m\nu > .1$ for our data, we expect the K_S^o yield we measure to be due predominantly to the valence d quark of the proton. The agreement in the z dependence of the K_S^o spectrum for these two experiments indicates that the fragmentation function for strange quarks into K_S^o's must have the same qualitative z dependence as that for d quarks.

In Fig. 19 we present the transverse momentum distribution for K_S^o's. The data are described nicely by an exponential in $p_\perp^2$ with a slope of 2.9 GeV^{-2}. This corresponds to an average $p_\perp$ of approximately 520 MeV. As is the case for charged hadrons, this average $p_\perp$ does not depend on Q^2 (see Fig. 20a). In Fig. 20b we have plotted the average $p_\perp$ versus z. The data is consistent with either no z dependence or with an increase of $\langle p_\perp \rangle$ with increasing z, similar as observed for charged hadrons (see section 4).

As expected, most Λ's are produced in the target fragmentation region as the Feynman x_F distribution in Fig. 21 shows. The invariant cross section for protons has been shown to be approximately independent of x_F for $x_F < 0,^5$ and our data seem to indicate a similar behavior for Λ's except in the very backward direction. The falloff in the backward direction may be due to poor efficiency for detecting slow Λ's. Further study is needed to understand if this is the case.

The transverse momentum distribution for Λ's is exponential in $p_\perp^2$ with a slope of 3.1 GeV^{-2} corresponding to an average $p_\perp$ of 500 MeV (see Fig. 22). This average $p_\perp$ is consistent with that measured for K^o's and is independent of Q^2 and x_F as shown in Fig. 23. The $p_\perp^2$ dependence for protons has previously been measured[20] and when fit with an exponential has a slope of approximately 4 GeV^{-2} as compared to the 3.1 ± 0.3 GeV^{-2} which we measure for Λ's.

Except for this apparent difference in transverse momentum dependence, the electroproduction of K^o's and Λ's is qualitatively the same as for other electroproduced hadrons. The transverse momentum distributions are independent of Q^2. In addition, the average transverse momentum of both strange and nonstrange mesons observed in electroproduction at high z, is larger than the typical $\langle p_\perp \rangle$ observed in hadronic reactions.

6. Inclusive ρ^o Production

Fig. 24a shows the effective mass spectrum for all $\pi^+\pi^-$ systems produced with $z > 0.6$, for $1 < Q^2 < 6$ GeV^2 and $2.5 < W < 4.2$ GeV. All hadrons were assumed to be pions. This leads to a bias in the background, but not in the ρ^o signal. Some of the ρ^o observed come from the "elastic" diffractive process $ep \to ep\rho^o$ which is eliminated by excluding all events which can be fit to the reaction $ep \to ep\pi^+\pi^-$. This results in Fig. 24b. One still sees a clear ρ^o signal.

The effective mass spectra were fitted by a superposition of a smooth background and a Breit-Wigner function for the ρ^o. For the background, a form $\sum_{k=-2}^{1} a_k (m_{\pi\pi})^k$ with fitted coefficients a_k was used. Similar fits were also made for other ranges of z of the $\pi\pi$ systems. The results for "inelastic" ρ^o production, expressed as a ratio of the number of ρ^o to the total number of negative hadrons observed (presumably nearly all π^-), may be summarized as follows:

in	$0.6 < z < 1.0$	we find $N^{\rho^o}(z_\rho)/N^{\pi^-}(z_\pi)$	~1.2
	$0.3 < z < 0.6$		~0.4
	$0 < z < 0.3$		~consistent with 0

These numbers are uncertain to within 30 % because the strong background under the ρ^o needs a more careful and detailed analysis. We note that for real photoproduction in the range of W from 2.5 to 4.3, a ratio of $N^{\rho^o}/N^{\pi^-} \sim 0.25$ has been reported.[21]

7. Charge Retention

From the quark-parton model one expects that for x increasing from 0 towards larger values an increasing amount of the net electric charge of the final hadronic state should be found in the quark fragmentation region. This happens

because the interaction with the current is increasingly dominated by u quarks. In the limiting case of only u quarks interacting and at sufficiently high energies the charge observed in the quark fragmentation region should be between +2/3 (for an SU(3) symmetric sea) or +1/2 (SU(2) symmetric sea).[22] Although at our energies we are nowhere near to observing a rapidity plateau, we nevertheless find an effect of the kind expected.

We use the energy range $2.5 < W < 4.2$ GeV and define the quark fragmentation region somewhat arbitrarily by $z > 0.3$. Fig. 25a shows the net hadronic electric charge observed in the two regions $0 < z < 0.3$ and $0.3 < z < 1$ as a function of x. The charge in the large-z region is seen to increase from small values for quarks in the sea region ($x \lesssim 0.1$), towards ~1/2 for x values between 0.3 and 0.5.

Charge retention is more properly studied in the current-quark Breit system. We cannot do this in a strict sense since in order to transform the hadrons into the Breit frame we would have to know their energies. We have estimated these by assuming all negatives to be pions, and assigning the pion or proton mass to the positives on a statistical basis, taking as a guideline π^+ and p distributions measured in other electroproduction experiments.[5,23] This procedure leads to Fig. 25b, which shows the total charge moving forward and backward, respectively, in the Breit frame as a function of x. The forward moving charge is again seen to increase strongly with increasing x, reaching a value of ~1/2 at $x = 0.4$.

Acknowledgements

We gratefully acknowledge the support of Professors Boyce McDaniel, H. Schopper and G. Weber and the staffs of the Wilson Synchrotron Laboratory and of DESY. We also thank E. Bassler, D. Dimakos, B. Hildebrandt, I. Hildebrandt, H. Neumann, F. Selonke, H. Siegner and I. Zank for their efforts in programming and in the scanning and measuring of the events. We would also like to acknowledge the contribution of John Seeman in the early stages of the experiment.

References

1. E. Albini et al., Nuovo Cimento A32, 101 (1976), and other references given in this compilation.
2. S.J. Brodsky and J.F. Gunion, Proceedings of the VII International Colloquium on Multiparticle Reactions, Tutzing, Germany (1976), p.369
3. R.P. Feynman, Photon-Hadron-Interactions, W.A. Benjamin, Inc. (1972)
4. S. Stein et al., Phys. Rev. D12, 1884 (1975)
5. C.J. Bebek et al., Phys. Rev. D15, 3077 (1977); Phys. Rev. Letters 32, 27 (1974); Phys. Rev. Letters 34, 1115 (1975)
6. H.L. Anderson et al., "Hadron Production in Muon-Proton and Muon-Deuteron Collisions", submitted to this conference
7. L.M. Sehgal, Nucl. Phys. B90, 471 (1975)
8. Ch. Berger et al., "Electroproduction of Neutral Pions and Test of the Quark-Parton Model", submitted to this conference
9. R. Brandelik et al., DESY preprint 77/11 (1977), and private communication from G. Wolf
10. H. Meyer (PLUTO), private communication
11. R.D. Field and R.P. Feynman, Phys. Rev. D15, 2590 (1977)
12. J.T. Dakin et al., Phys. Rev. D10, 1401 (1974)
13. H.L. Anderson et al., Phys. Rev. Letters 36, 1422 (1976)
14. J.W. Chapman et al., Phys. Rev. D14, 5 (1976)
15. C. del Papa et al., Phys. Rev. D15, 2425 (1977)
16. J.P. Berge et al., preprint FNAL-PUB 75/84 EXP
17. G. Hanson et al., Phys. Rev. Letters 35, 1609 (1975)
18. R.P. Feynman, R.D. Field, and G.C. Fox, preprint CALT-68-595 (1977)
19. J. Burmester et al., DESY preprint 77/14 (1977)
20. K.M. Hanson, Proceedings of the 1975 International Symposium on Lepton and Photon Interactions at High Energies (W.T. Kirk, Ed.), Stanford University, August 1975, p.739

21. E. Kogan et al., Nucl. Phys. B122, 383 (1977)

22. S.J. Brodsky and N. Weiss, preprint SLAC-PUB-1926 (1977)

23. J.C. Alder et al., Nucl. Phys. B46, 415 (1972)

24. K.C. Moffeit et al., Phys. Rev. D5, 1603 (1972)

25. C.K. Chen et al., "Charged Hadron Multiplicities and Inclusive π^- Distributions in Inelastic ep-Scattering", submitted to this conference.

26. D.C. Horn et al., Phys. Rev. Letters 37, 1374 (1976)

Figure captions

Fig. 1 Schematic top (a) and side view (b) of the experiment. The electron beam enters from the left. The trigger uses a coincidence of scintillation counters behind the streamer chamber ("STREAMER COUNTERS"), with a hodoscope, a lead-lucite sandwich counter ("SAND"), a scintillation counter array near the shower maximum ("PEAK") and a lead-perchlorate shower counter ("TANK"). The "TAG" counters (scintillation and shower counters below the beam) served to detect electrons that have lost energy by producing bremsstrahlung in the target.

Fig. 2 The mean charged hadron multiplicity as a function of Q^2 in various regions of the total hadronic mass W. The photoproduction points shown for comparison are from Ref. 24.

Fig. 3 The mean charged hadron multiplicity for $1 < Q^2 < 6$ GeV^2 as a function of the squared mass of the hadronic system.

Fig. 4 The mean charged hadron multiplicity $\langle n_{ch} \rangle_z$ as a function of fractional momentum $z = p_h/\nu$ of one of the charged hadrons. The curve is explained in the text. Only events in the region $Q^2 > 1$ GeV^2 were used.

Fig. 5 The sum of positive and negative hadrons vs. $z = P_h/\nu$ for different regions of Q^2 and $x' = Q^2/(Q^2 + W^2)$. All events with W greater than 1.8 GeV are included in this plot.

Fig. 6 The sum of positive and negative hadrons vs. $z = P_h/\nu$ for different regions of $x = Q^2/2m\nu$. W is required to be greater than 3 GeV.

Fig. 7 The multiplicity at high $z = P_h/\nu$ versus W^2 for two Q^2 regions. The point at 100 GeV^2 is from Ref. 6. The dashed line represents an estimate of our data with proton contamination removed.

Fig. 8 The multiplicity at high $z = P_h/\nu$ versus $x' = Q^2/(Q^2 + W^2)$ for narrow W^2 bins. Only data with $Q^2 > 1$ GeV^2 are used.

Fig. 9 The difference of positive and negative hadrons vs. $z = p_h/\nu$ for several regions of $x = Q^2/2m\nu$. W is required to be greater than 3 GeV. The data for the three different x regions have arbitrary relative normalization since only the shapes of the z distributions are to be compared.

Fig. 10 Comparison of our measured hadron distribution as a function of $z = P_h/\nu$, with other recent data from electroproduction and e^+e^- annihilation. Previous work from eN, νN and e^+e^- is summarized by the band indicating the fits by Field and Feynman (Ref. 11) to these data. (The data shown from our experiment are from events with $Q^2 > 1$ GeV^2, $W^2 > 12$ GeV^2, and $x = Q^2/2m\nu > 0.1$.)

Fig. 11 Quark fragmentation functions for positive and negative pions as a function of $z = p_\pi/\nu$. Only events with $Q^2 > 1$ GeV^2, $W^2 > 12$ GeV^2, and $x = Q^2/2m\nu > 0.1$ are used.

Fig. 12 The distribution of the square of transverse momentum of the charged hadrons, for total hadronic mass in the range $3.0 < W < 4.2$ GeV and for various regions in Q^2 and $z = p_h/\nu$.

Fig. 13 The dependence of the average transverse momentum of the charged hadrons on Q^2, $x = Q^2/2m\nu$, and W, separately for two ranges of $z = p_h/\nu$.

Fig. 14 The dependence of the average transverse momentum of the charged hadrons on their fractional momentum $z = p_h/\nu$, for $1 < Q^2 < 6$ GeV^2 and various regions of the total hadronic mass W.

Fig. 15a The dependence of the average transverse momentum of the charged hadrons on $x = Q^2/2m\nu$, for $1 < Q^2 < 6$ GeV^2 and various regions of the total hadronic mass W.

Fig. 15b The dependence of the average transverse momentum for negative hadrons on W, for events with $Q^2 > 1$ GeV^2 in various bins of Feynman's scaling variable $x_F = p^*_{h\parallel}/p^*_{h\ max}$. (The momenta are taken in the cms of the current and the target proton.)

Fig. 16 The ratio of the numbers of positive and negative hadrons as a function of their squared transverse momentum, for $1 < Q^2 < 6$ GeV^2, $2.5 < W < 4.2$ GeV and various regions of $x = Q^2/2m\nu$.

Fig. 17 Proton$-\pi^-$ and $\pi^+-\pi^-$ mass distributions. See the text for details of event selection.

Fig. 18 Comparison of the z distributions of K^o_S produced in colliding beam experiments and in electron scattering. The definitions of z apply to electroproduction and colliding beam experiments respectively.

Fig. 19 The transverse momentum distribution for electroproduced K^o_S's.

Fig. 20 The average transverse momentum for electroproduced K^o_S's vs a) Q^2 and b) z.

Fig. 21 The Feynman x_F distribution for electroproduced Λ's.

Fig. 22 The transverse momentum distribution for electroproduced Λ's.

Fig. 23 The average transverse momentum for electroproduced Λ's vs a) Q^2 and b) x_F.

Fig. 24 The effective mass spectra of $\pi^+\pi^-$ systems produced with a fractional momentum $z = |\vec{p}_{\pi^+} + \vec{p}_{\pi^-}|/\nu > 0.6$.

Fig. 25 The net electric charge of all hadrons produced in the current and in the target regions, as a function of $x = Q^2/2m\nu$. These regions are defined (a) in terms of the fractional momentum $z = p_h/\nu$ (in the laboratory system), or (b) by forward or backward motion, respectively, in the current-quark Breit frame. Fig. 25b involves a separation of the various species of hadrons observed, which could be done only approximately (see text).

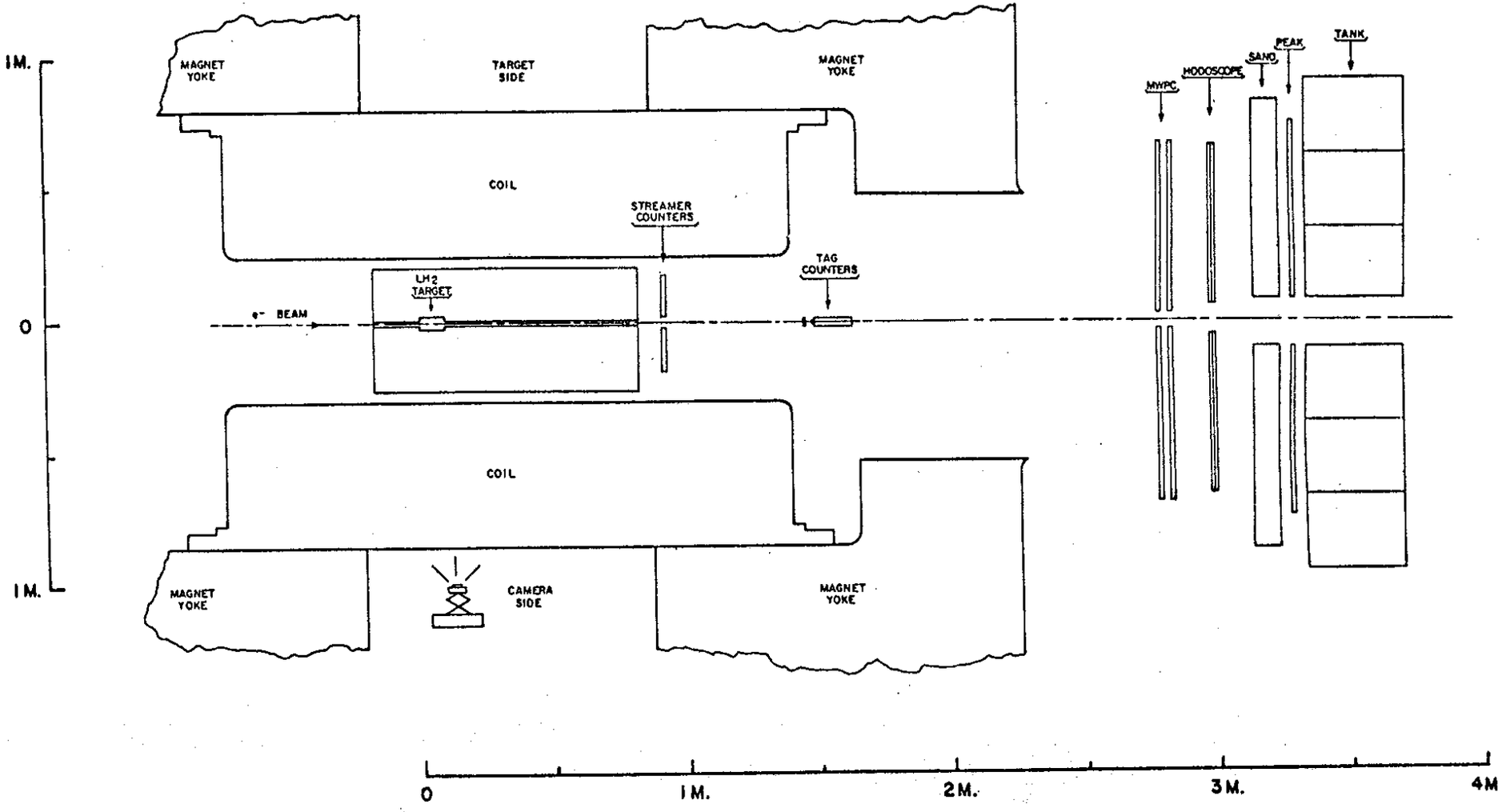

TOP VIEW

Fig. 1a

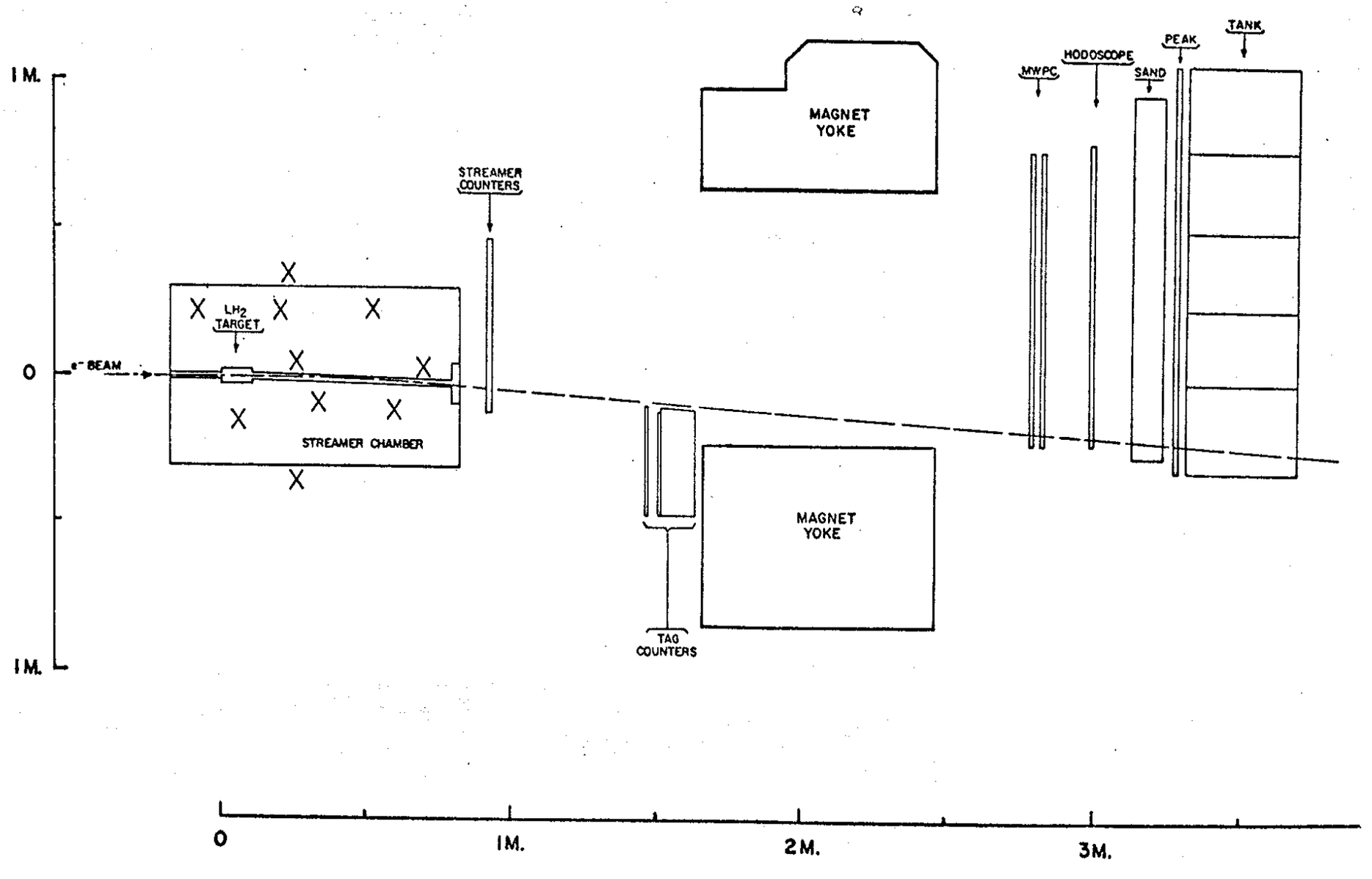

Fig. 1b

VIEW FROM CAMERA SIDE

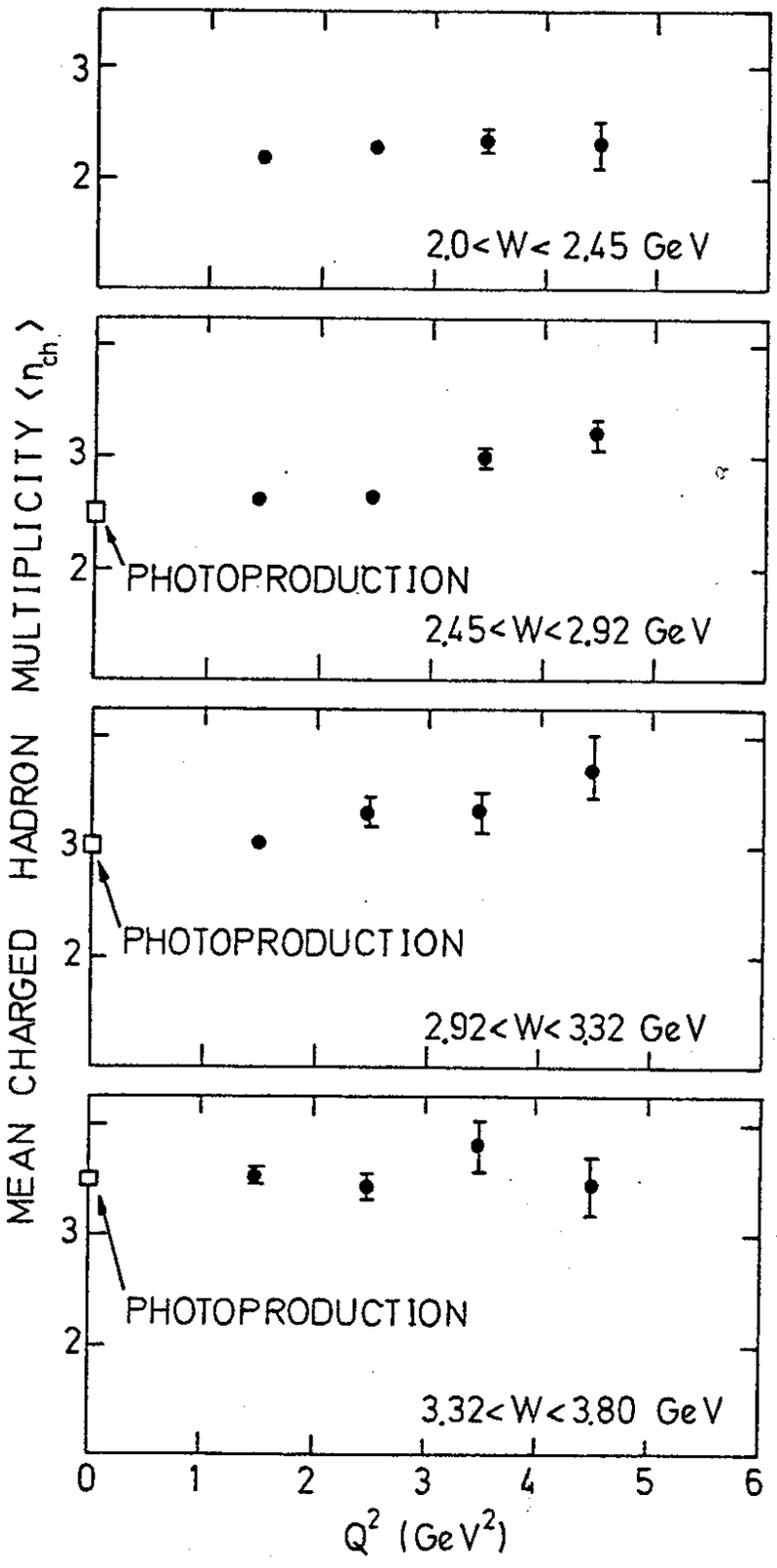
MEAN CHARGED HADRON MULTIPLICITY $\langle n_{ch} \rangle$
2.0< W< 2.45 GeV
PHOTOPRODUCTION
2.45< W< 2.92 GeV
PHOTOPRODUCTION
2.92< W< 3.32 GeV
PHOTOPRODUCTION
3.32< W< 3.80 GeV
Q^2 (GeV^2)

Fig. 2

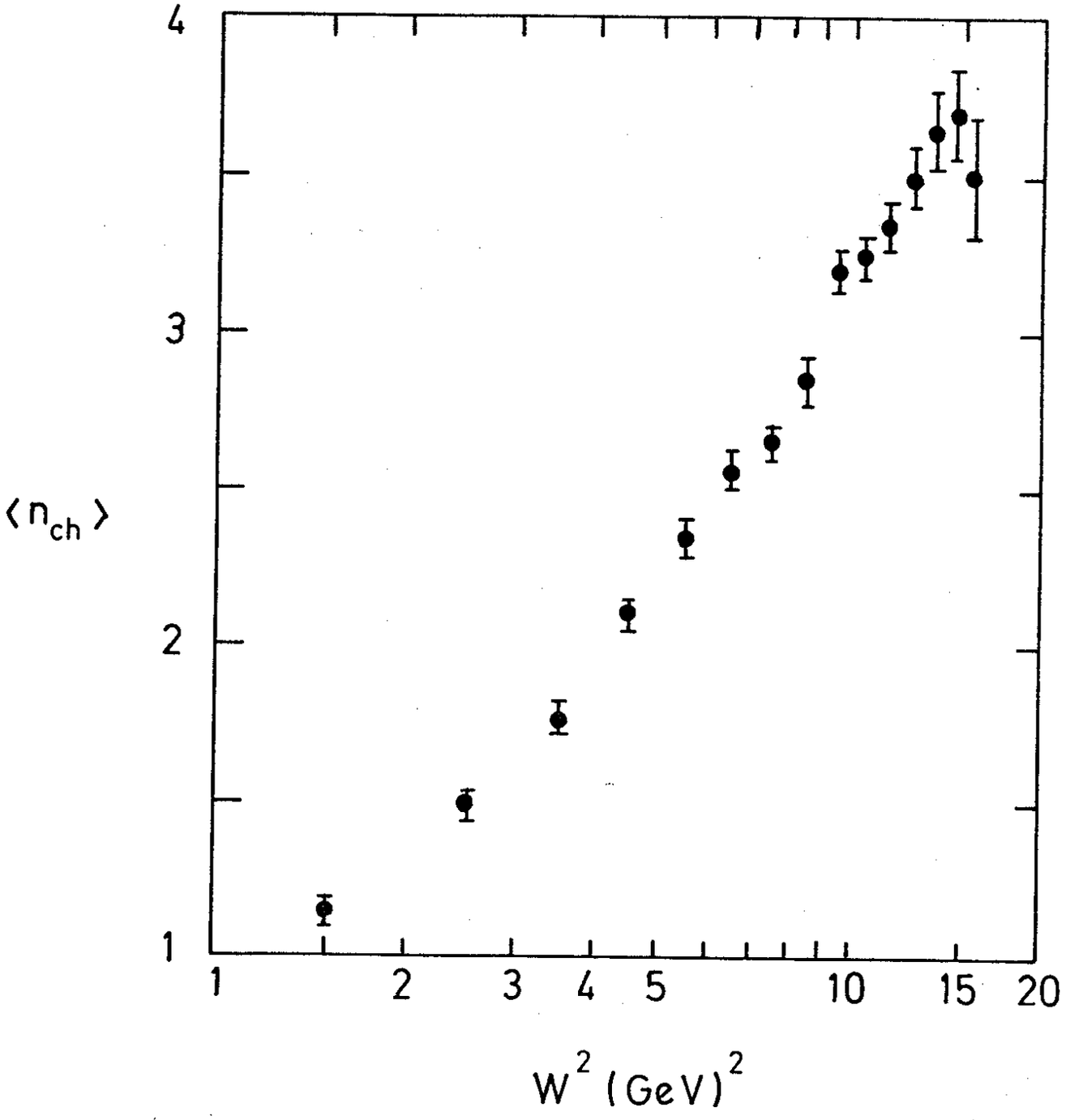
4
3
2
1
⟨ n_ch ⟩
1
2
3
4
5
10
15
20
W² (GeV)²

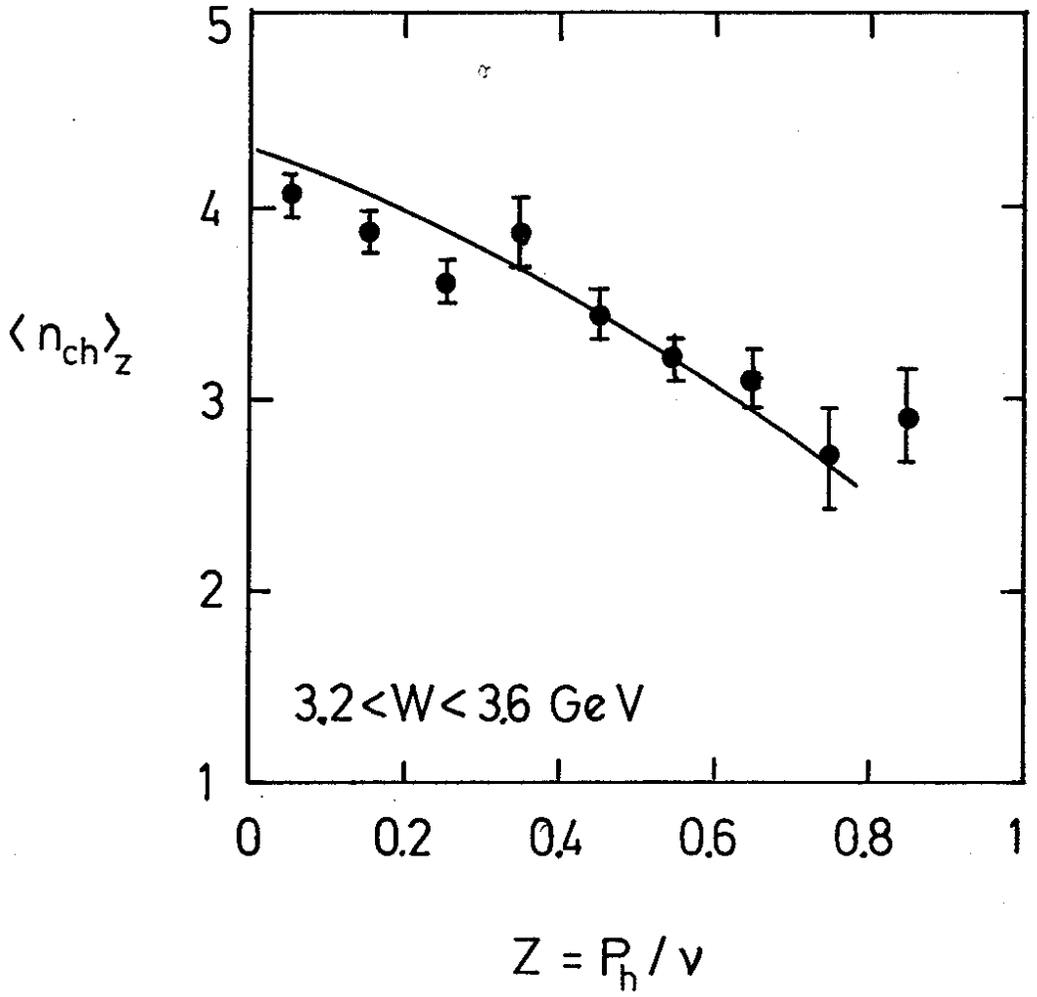

Fig. 4

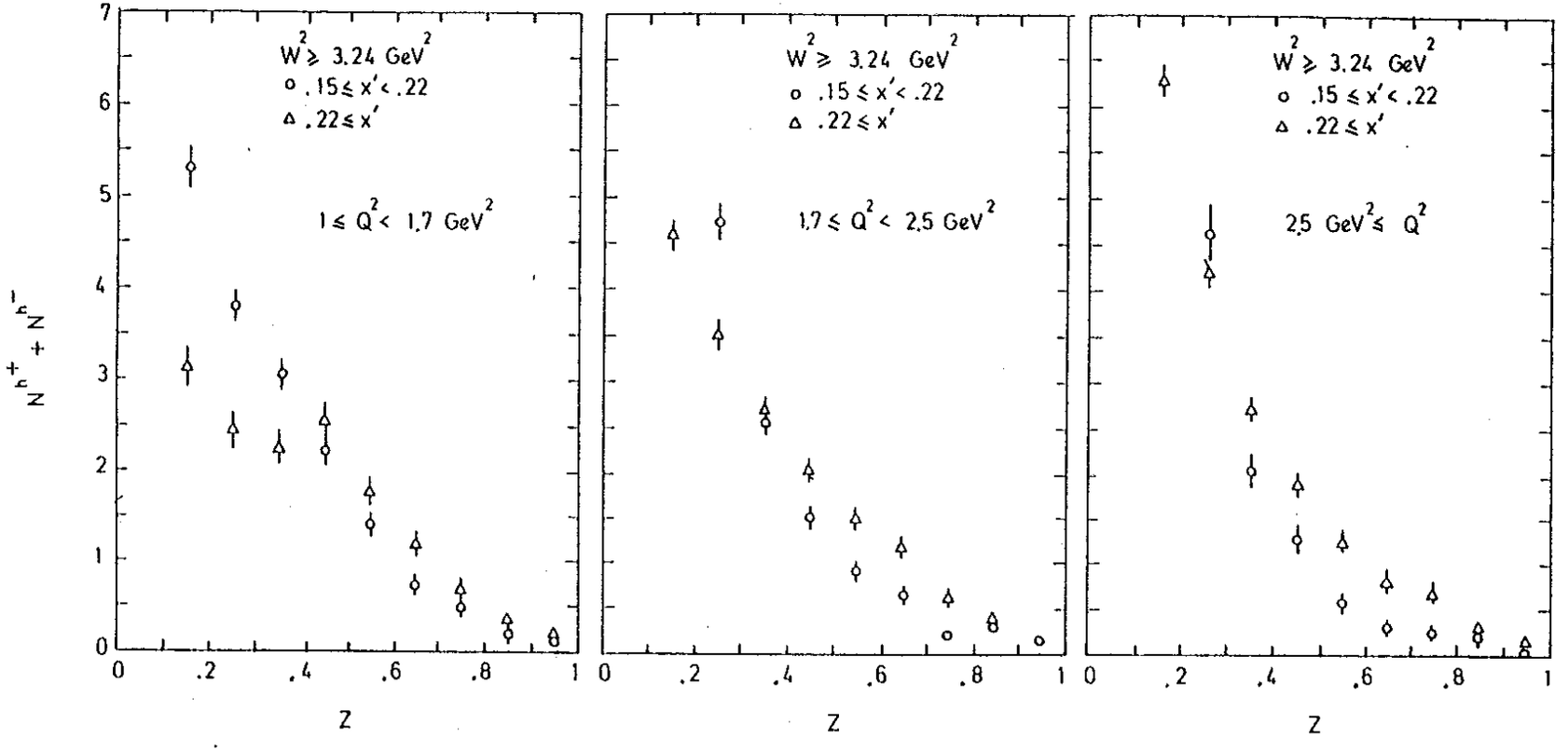
$W^2 \geq 3.24\ GeV^2$
o $.15 \leq x' < .22$
Δ $.22 \leq x'$
$1 \leq Q^2 < 1.7\ GeV^2$
$1.7 \leq Q^2 < 2.5\ GeV^2$
$2.5\ GeV^2 \leq Q^2$
$N^{\pi}_{1} + N^{\pi}_{-1}$
Z
0
.2
.4
.6
.8
1
2
3
4
5
6
7

Figure 5

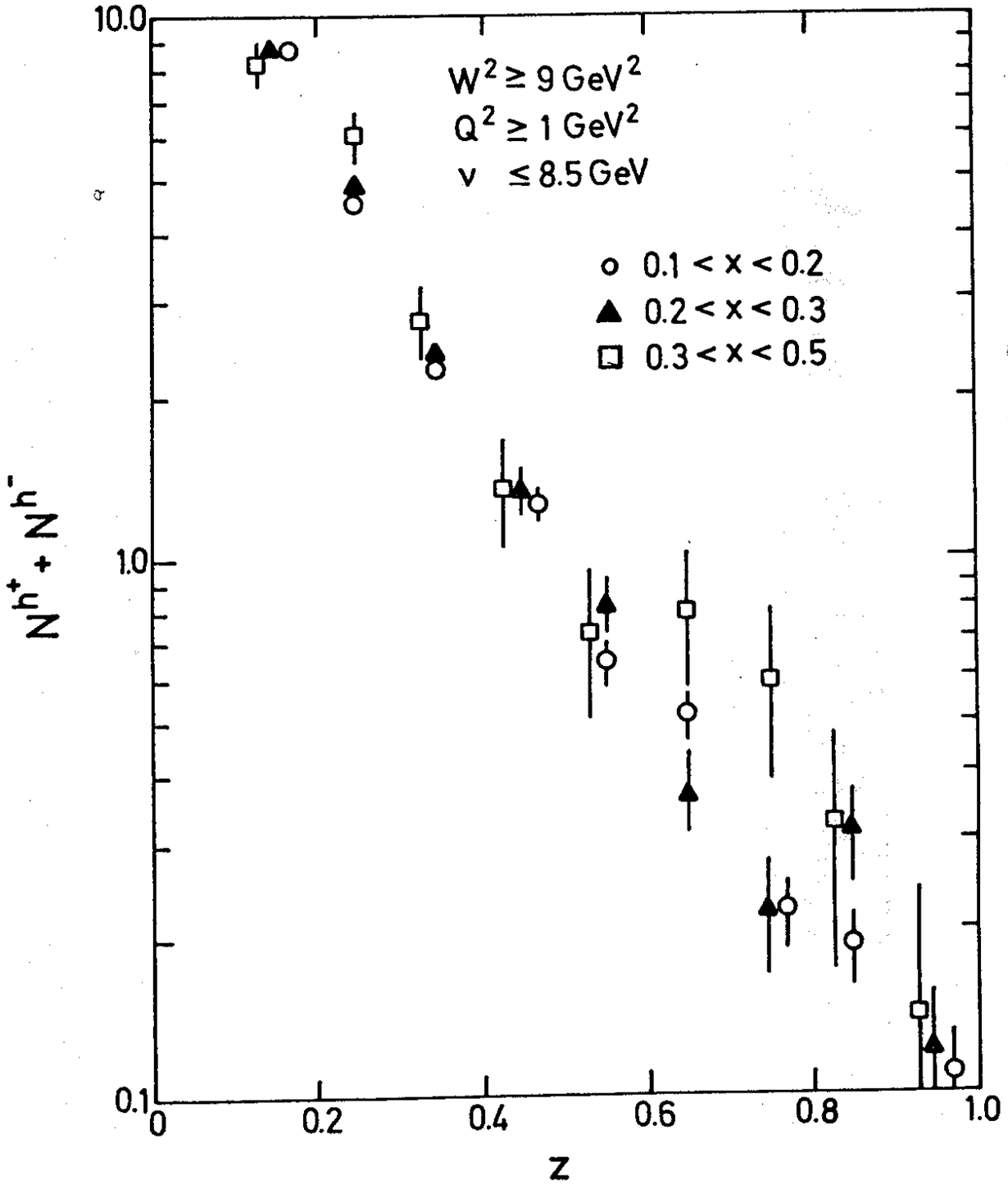
10.0
1.0
0.1
0
0.2
0.4
0.6
0.8
1.0
z
$N^{h^+} + N^{h^-}$
$W^2 \geq 9\,GeV^2$
$Q^2 \geq 1\,GeV^2$
$\nu \leq 8.5\,GeV$
$0.1 < x < 0.2$
$0.2 < x < 0.3$
$0.3 < x < 0.5$

Fig. 6

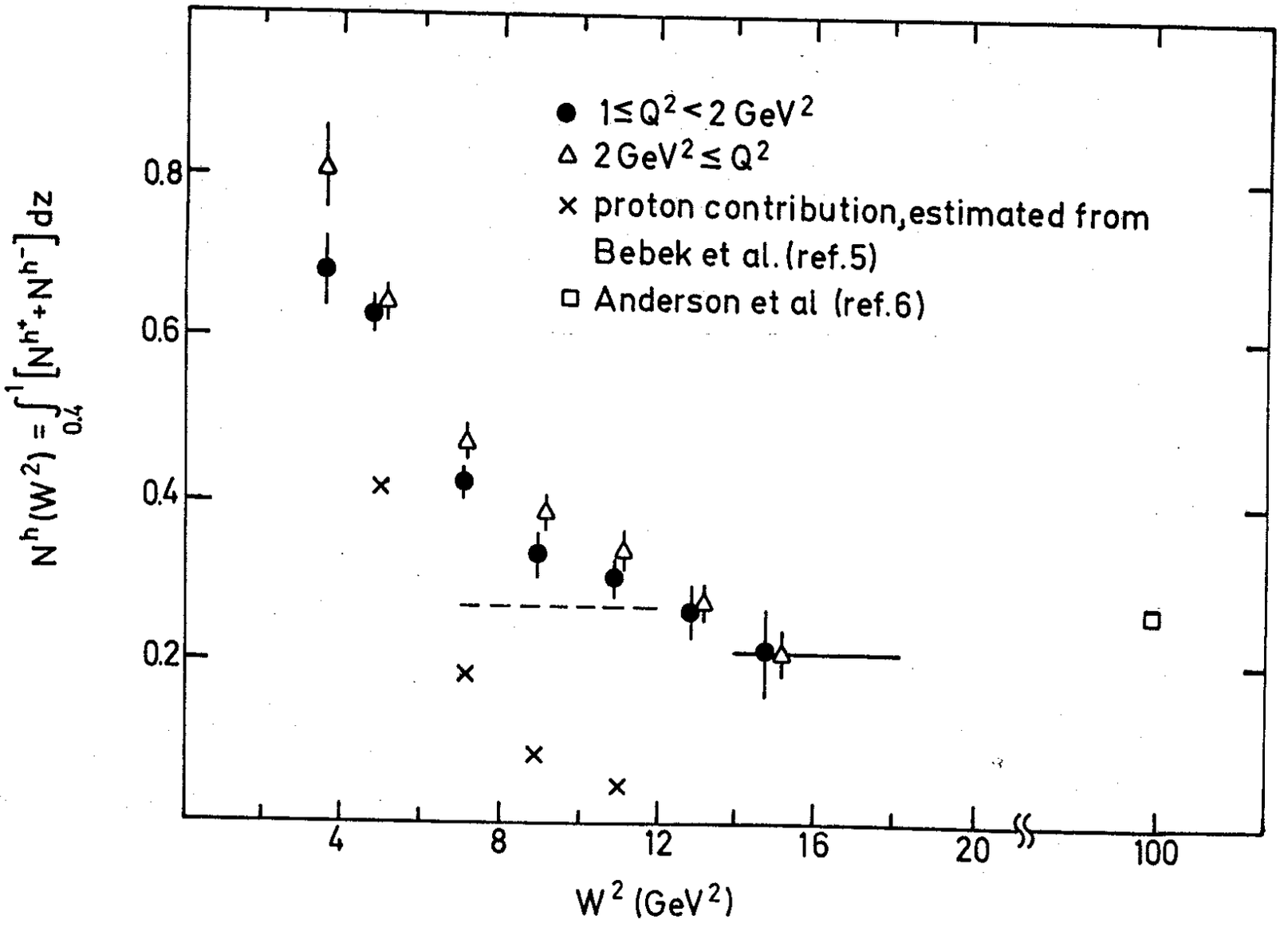
● 1≤Q²<2 GeV²
△ 2GeV²≤Q²
× proton contribution, estimated from Bebek et al. (ref.5)
□ Anderson et al (ref.6)
$N^h(W^2) = \int_{0.4}^{1} [N^{h^+} + N^{h^-}] dz$
0.8
0.6
0.4
0.2
4
8
12
16
20
100
W^2 (GeV²)

Figure 7

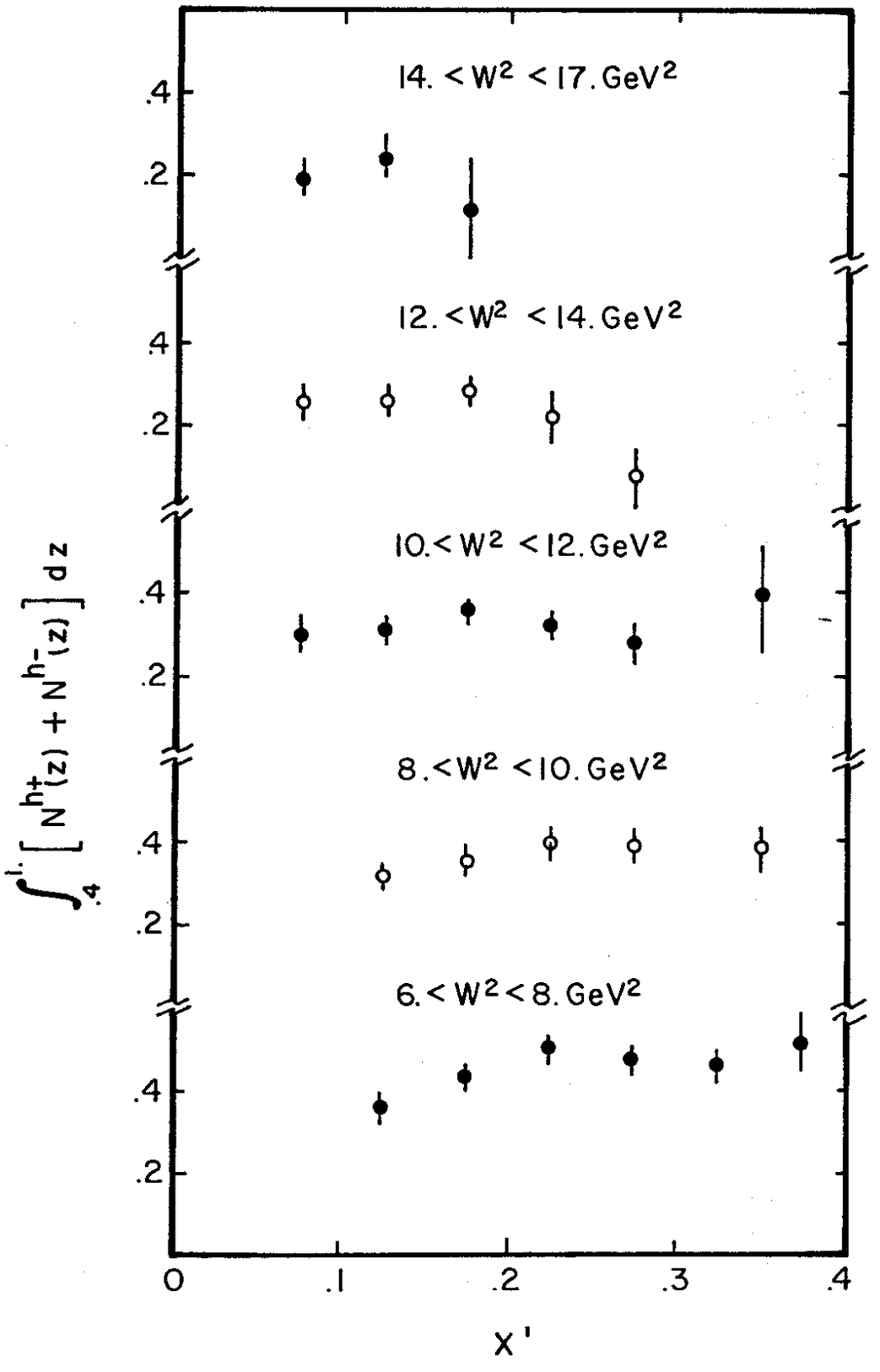
14. < W² < 17. GeV²
12. < W² < 14. GeV²
10. < W² < 12. GeV²
8. < W² < 10. GeV²
6. < W² < 8. GeV²
.4
.2
0
.1
.2
.3
.4
X'
$\int_{.4}^{1.} \left[N^{h^+}(z) + N^{h^-}(z) \right] dz$

Fig. 8

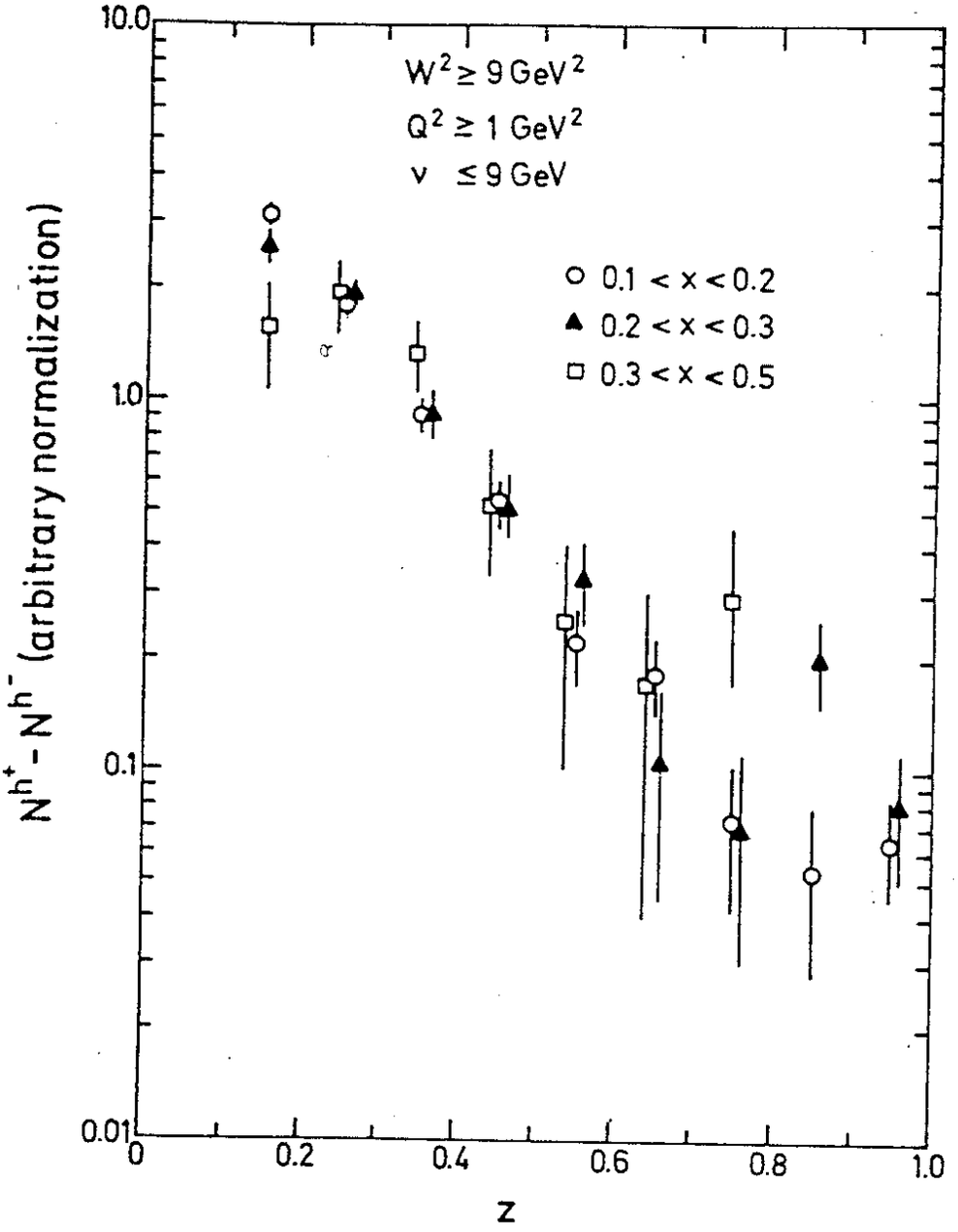
10.0
1.0
0.1
0.01
0
0.2
0.4
0.6
0.8
1.0
z
$N^{h^+} - N^{h^-}$ (arbitrary normalization)
$W^2 \geq 9\ GeV^2$
$Q^2 \geq 1\ GeV^2$
$\nu \leq 9\ GeV$
○ 0.1 < x < 0.2
▲ 0.2 < x < 0.3
□ 0.3 < x < 0.5

Fig. 9

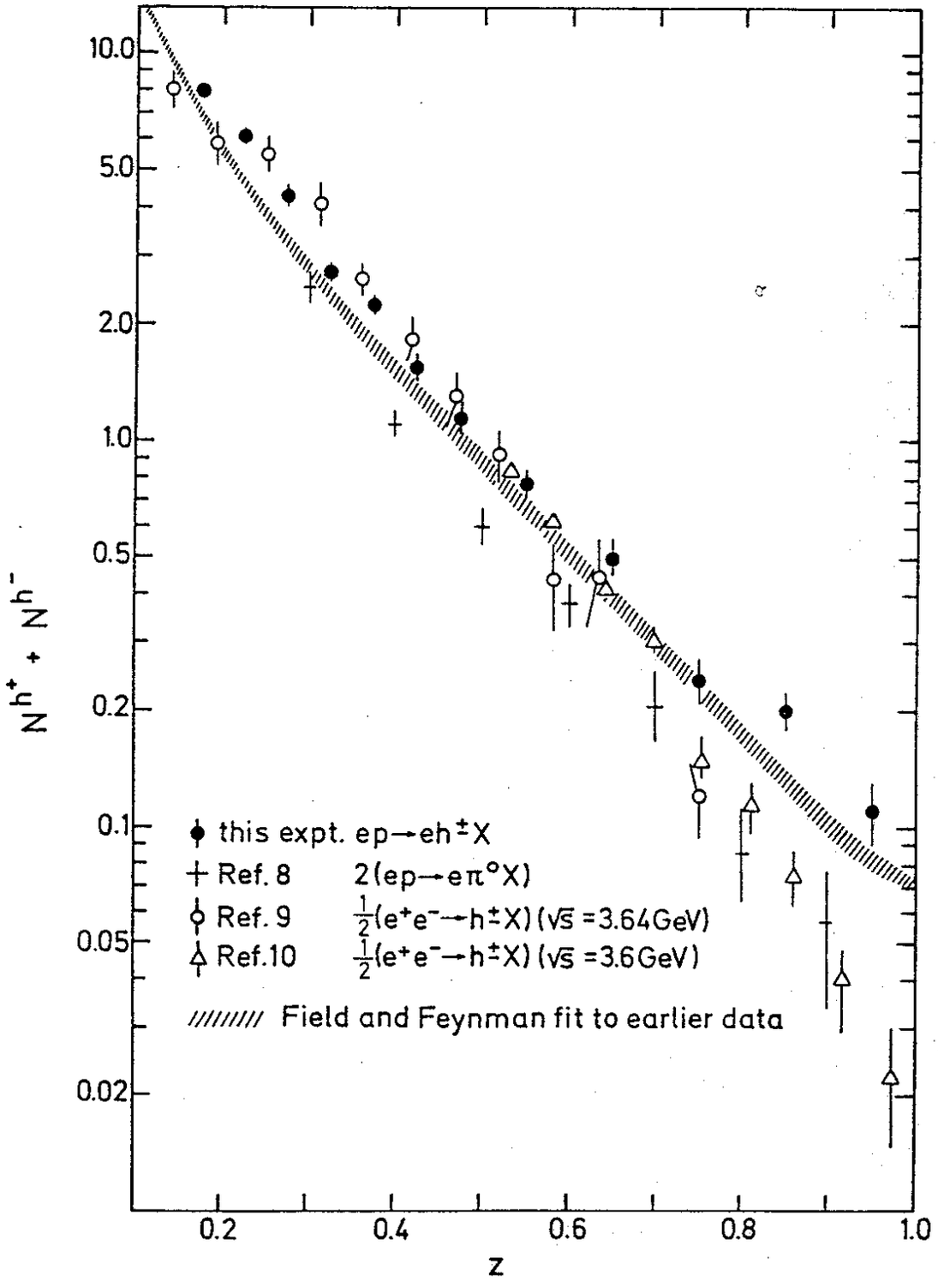
10.0
5.0
2.0
1.0
0.5
0.2
0.1
0.05
0.02
$N^{h^+} + N^{h^-}$
0.2
0.4
0.6
0.8
1.0
z
this expt. $ep \rightarrow eh^{\pm}X$
Ref. 8 $2(ep \rightarrow e\pi^{\circ}X)$
Ref. 9 $\frac{1}{2}(e^+e^- \rightarrow h^{\pm}X)$ ($\sqrt{s}$ = 3.64GeV)
Ref.10 $\frac{1}{2}(e^+e^- \rightarrow h^{\pm}X)$ ($\sqrt{s}$ = 3.6GeV)
Field and Feynman fit to earlier data

Figure 10

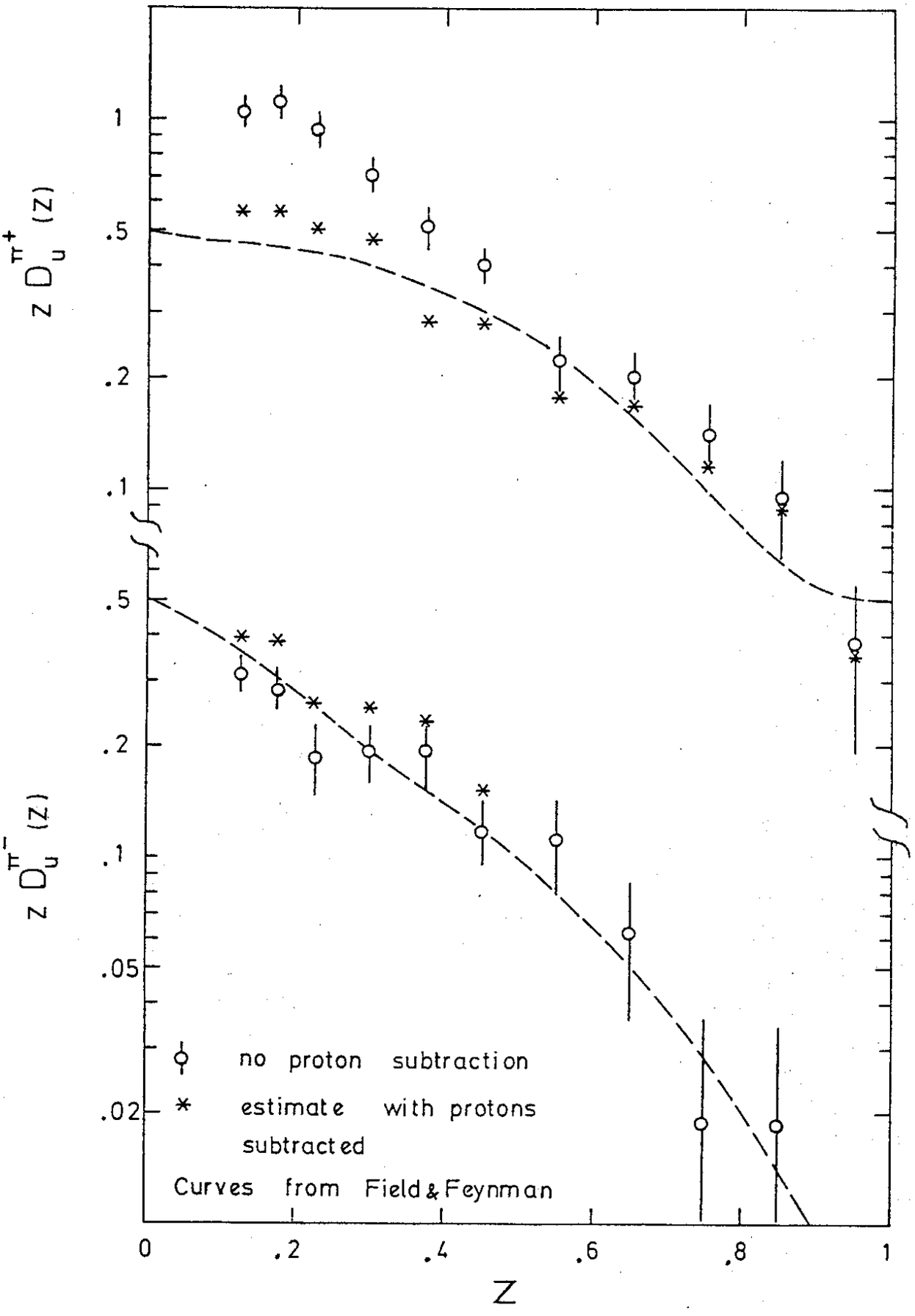
z D_u^π+ (z)
z D_u^π− (z)
1
.5
.2
.1
.5
.2
.1
.05
.02
no proton subtraction
estimate with protons subtracted
Curves from Field & Feynman
0
.2
.4
.6
.8
1
Z

Figure 11

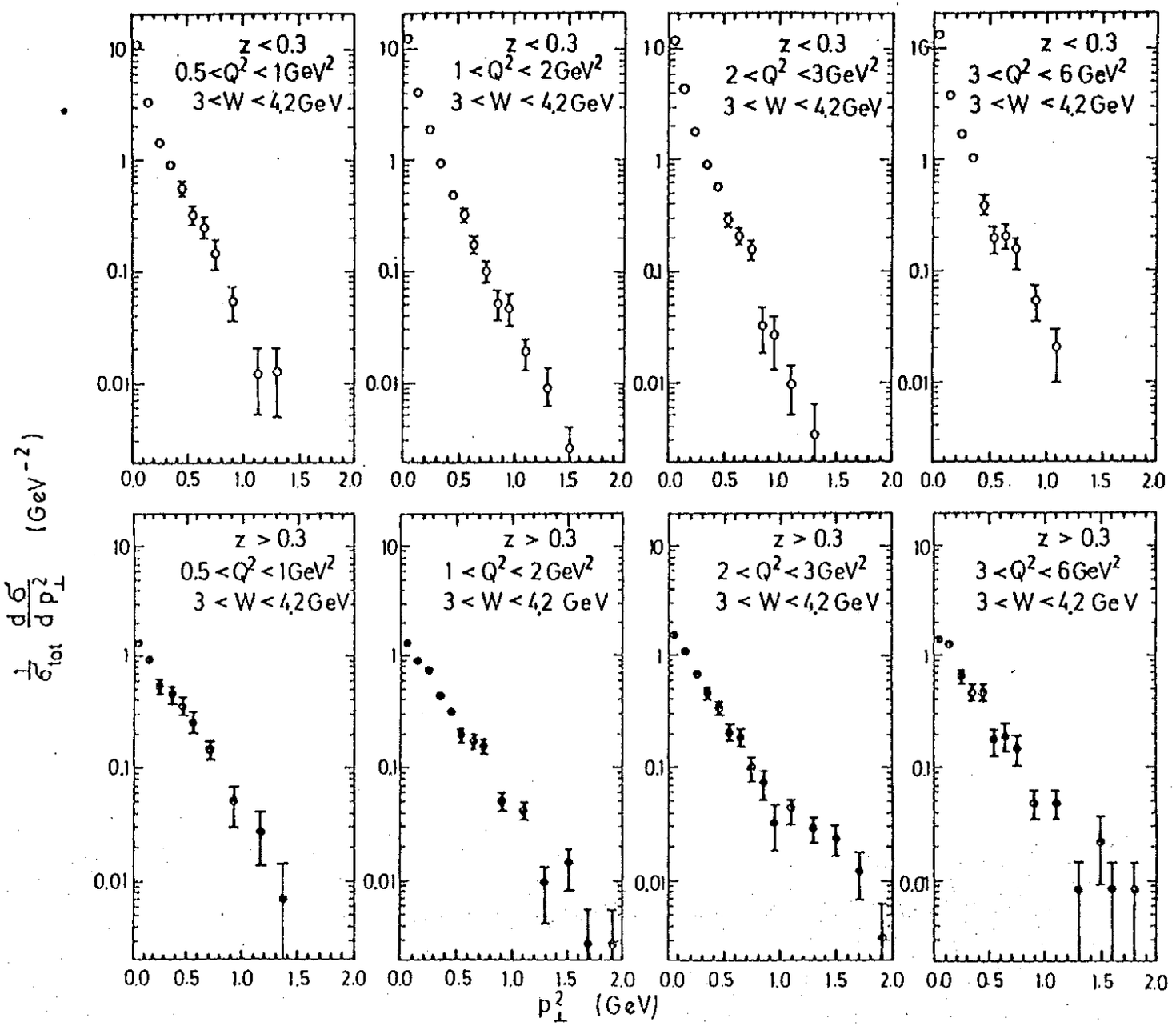
z < 0.3
0.5<Q² < 1GeV²
3<W < 4.2GeV
z < 0.3
1 < Q² < 2GeV²
3 < W < 4.2GeV
z < 0.3
2 < Q² < 3GeV²
3 < W < 4.2GeV
z < 0.3
3 < Q² < 6 GeV²
3 < W < 4.2GeV
z > 0.3
0.5 < Q² < 1GeV²
3 < W < 4.2GeV
z > 0.3
1 < Q² < 2 GeV²
3 < W < 4.2 GeV
z > 0.3
2 < Q² < 3GeV²
3 < W < 4.2 GeV
z > 0.3
3 < Q² < 6GeV²
3 < W < 4.2 GeV
$\frac{1}{\sigma_{tot}} \frac{d\sigma}{dp_\perp^2}$ (GeV^{-2})
$p_\perp^2$ (GeV)

Fig. 12

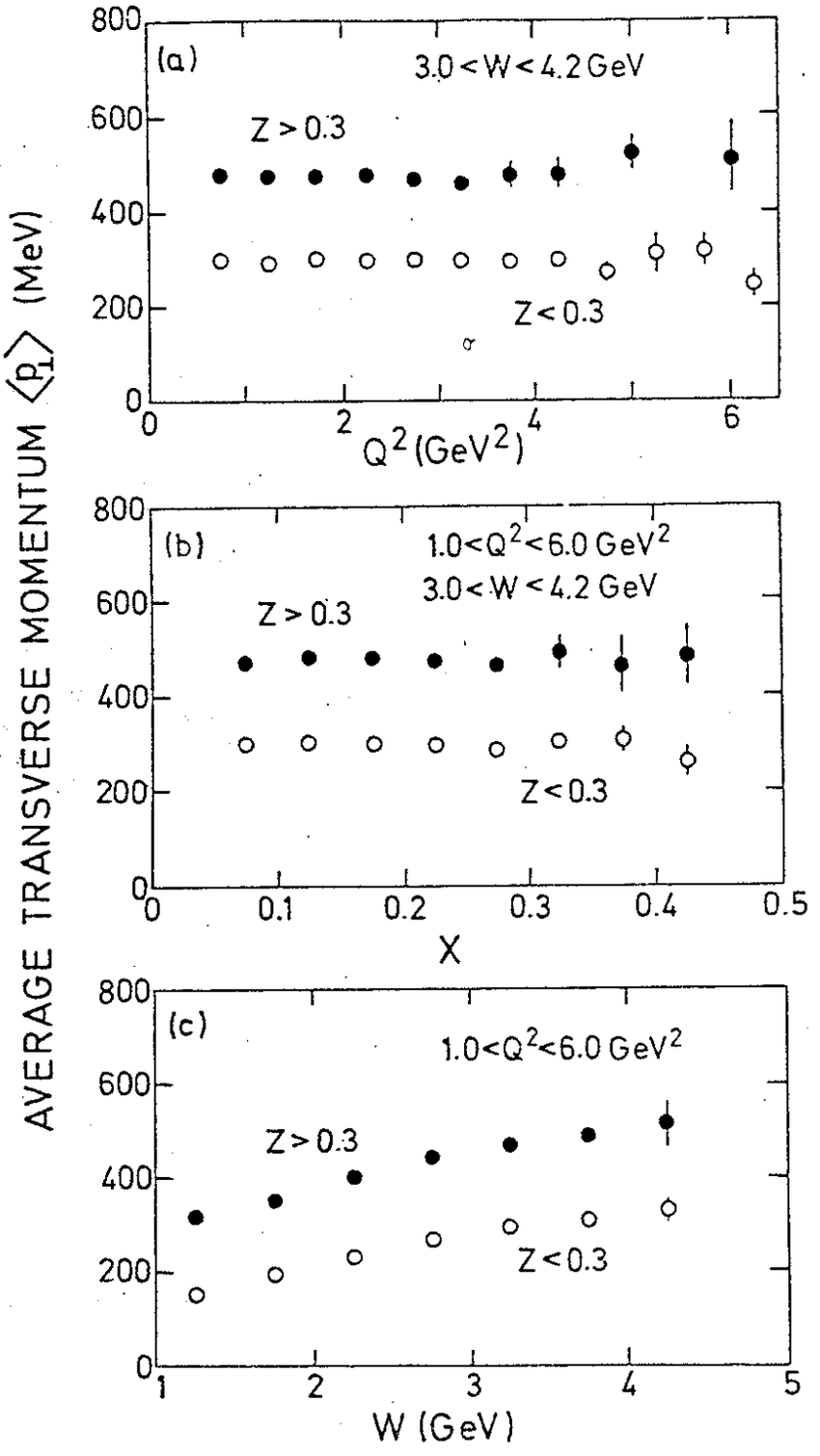
AVERAGE TRANSVERSE MOMENTUM $\langle p_T \rangle$ (MeV)
(a)
3.0 < W < 4.2 GeV
Z > 0.3
Z < 0.3
Q^2 (GeV^2)
(b)
1.0 < Q^2 < 6.0 GeV^2
3.0 < W < 4.2 GeV
Z > 0.3
Z < 0.3
X
(c)
1.0 < Q^2 < 6.0 GeV^2
Z > 0.3
Z < 0.3
W (GeV)

Fig. 13

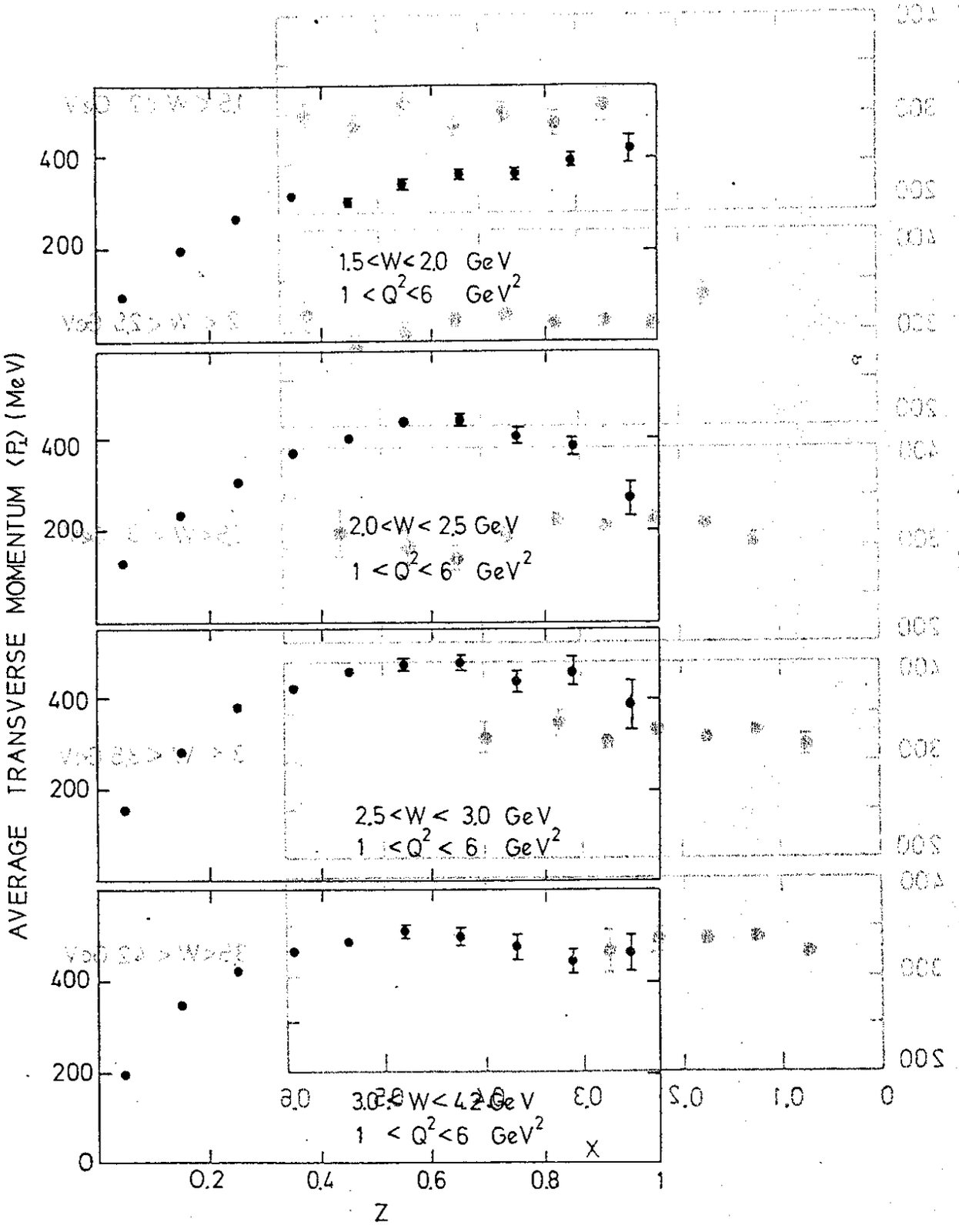
AVERAGE TRANSVERSE MOMENTUM ⟨P⊥⟩ (MeV)
400
200
0
1.5<W<2.0 GeV
1 <Q²<6 GeV²
2.0<W<2.5 GeV
1 <Q²<6 GeV²
2.5<W< 3.0 GeV
1 <Q²< 6 GeV²
3.0<W<4.2 GeV
1 <Q²<6 GeV²
0.2
0.4
0.6
0.8
1
Z
X

Fig. 14

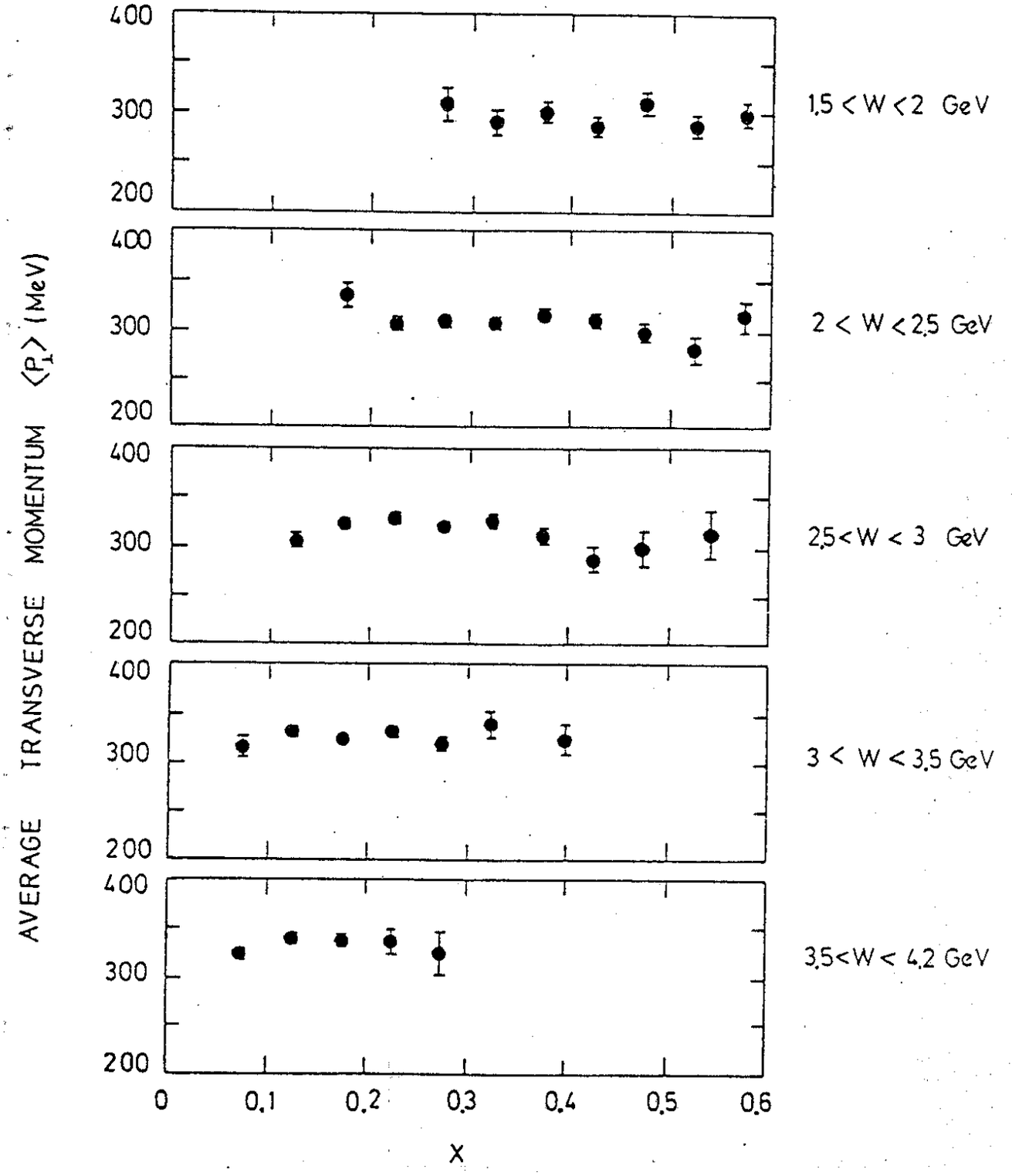
AVERAGE TRANSVERSE MOMENTUM ⟨P_T⟩ (MeV)
400
300
200
1.5 < W < 2 GeV
2 < W < 2.5 GeV
2.5 < W < 3 GeV
3 < W < 3.5 GeV
3.5 < W < 4.2 GeV
0
0.1
0.2
0.3
0.4
0.5
0.6
X

Fig. 15a

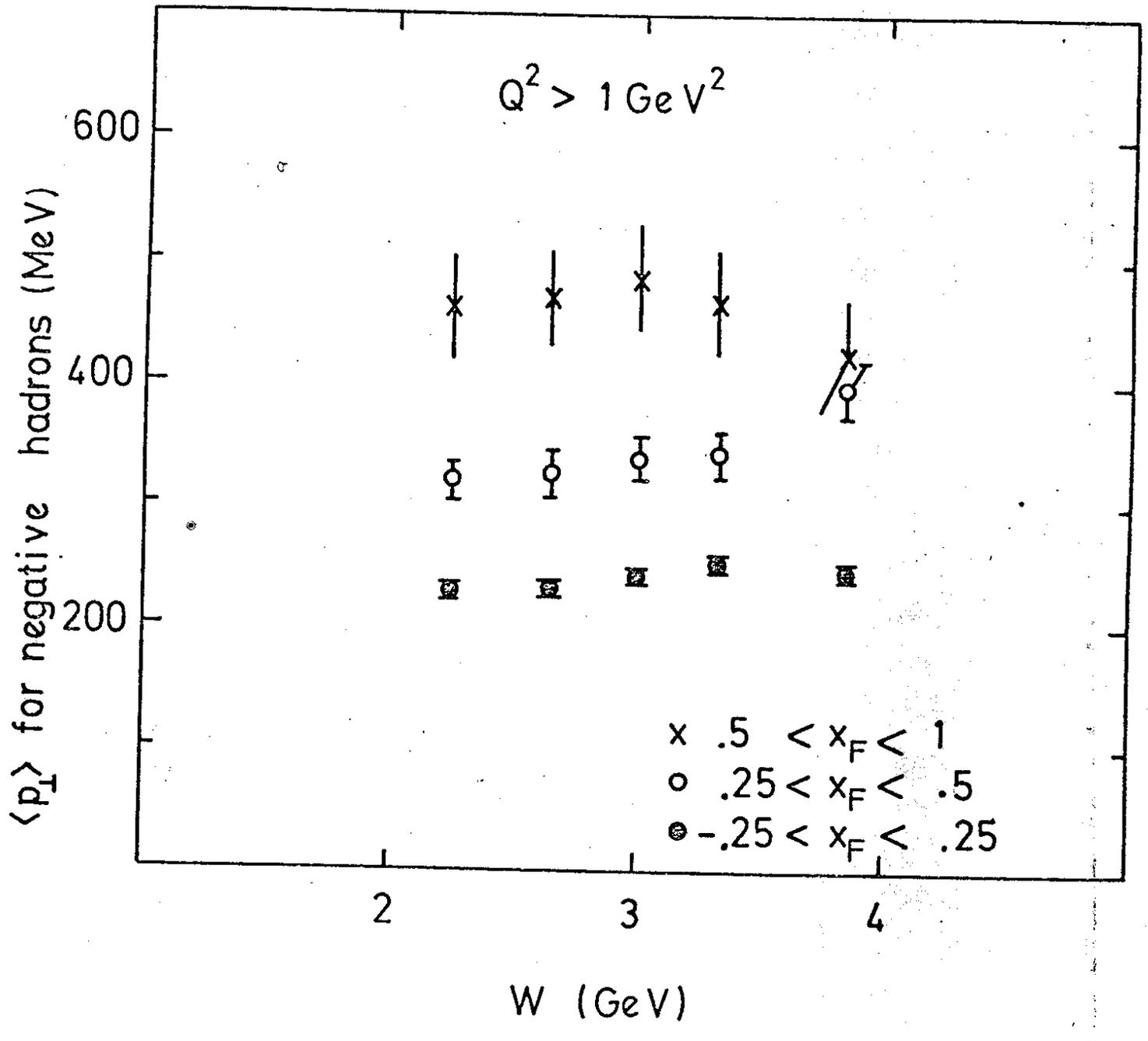
$Q^2 > 1\,GeV^2$
600
400
200
$\langle p_T \rangle$ for negative hadrons (MeV)
x .5 < x_F < 1
o .25 < x_F < .5
⊛ -.25 < x_F < .25
2
3
4
W (GeV)

Fig. 15b

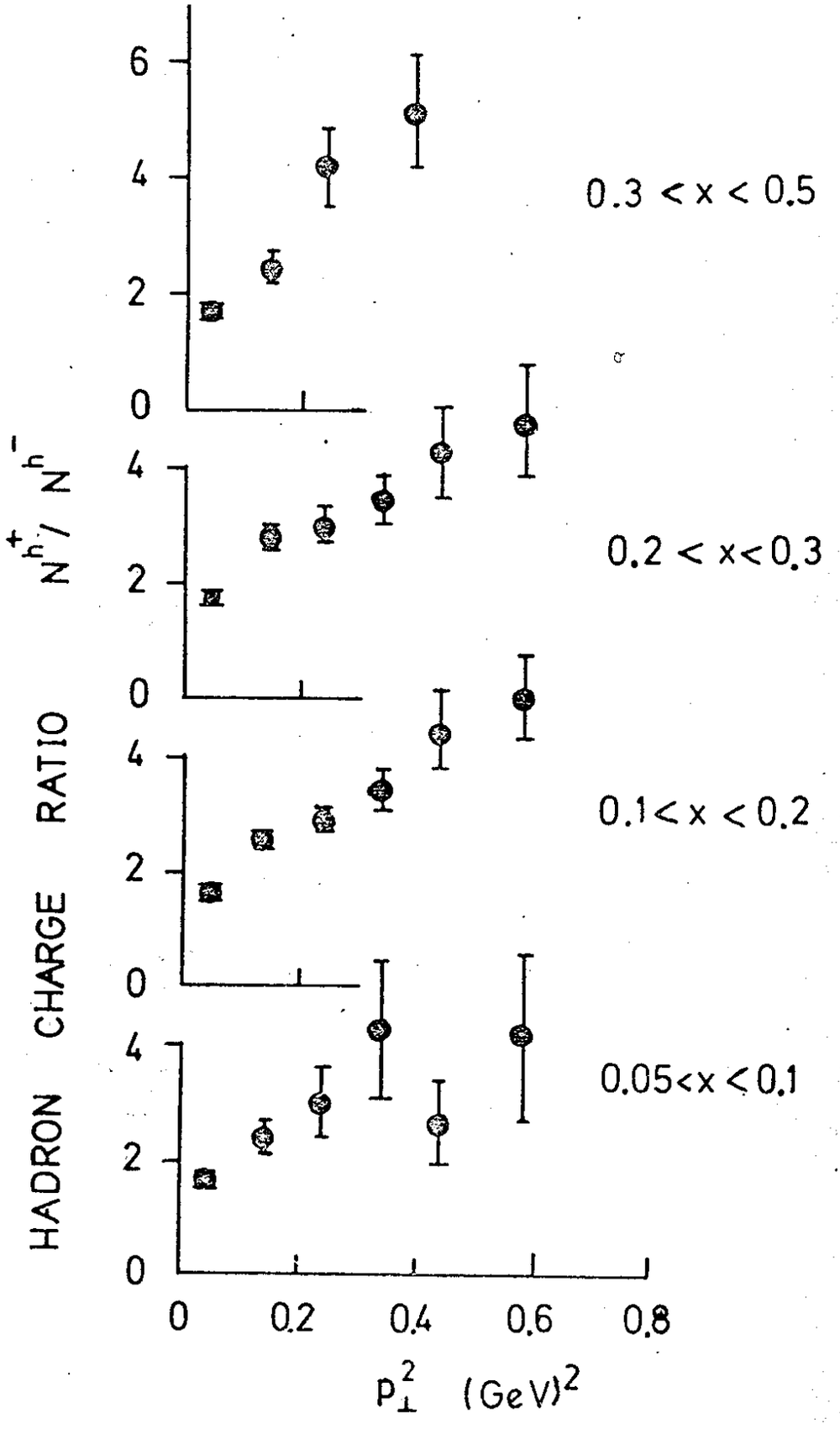
HADRON CHARGE RATIO
N^{h^+} / N^{h^-}
0.3 < x < 0.5
0.2 < x < 0.3
0.1 < x < 0.2
0.05 < x < 0.1
0
2
4
6
0
0.2
0.4
0.6
0.8
$p_\perp^2$ (GeV)^2

Fig. 16

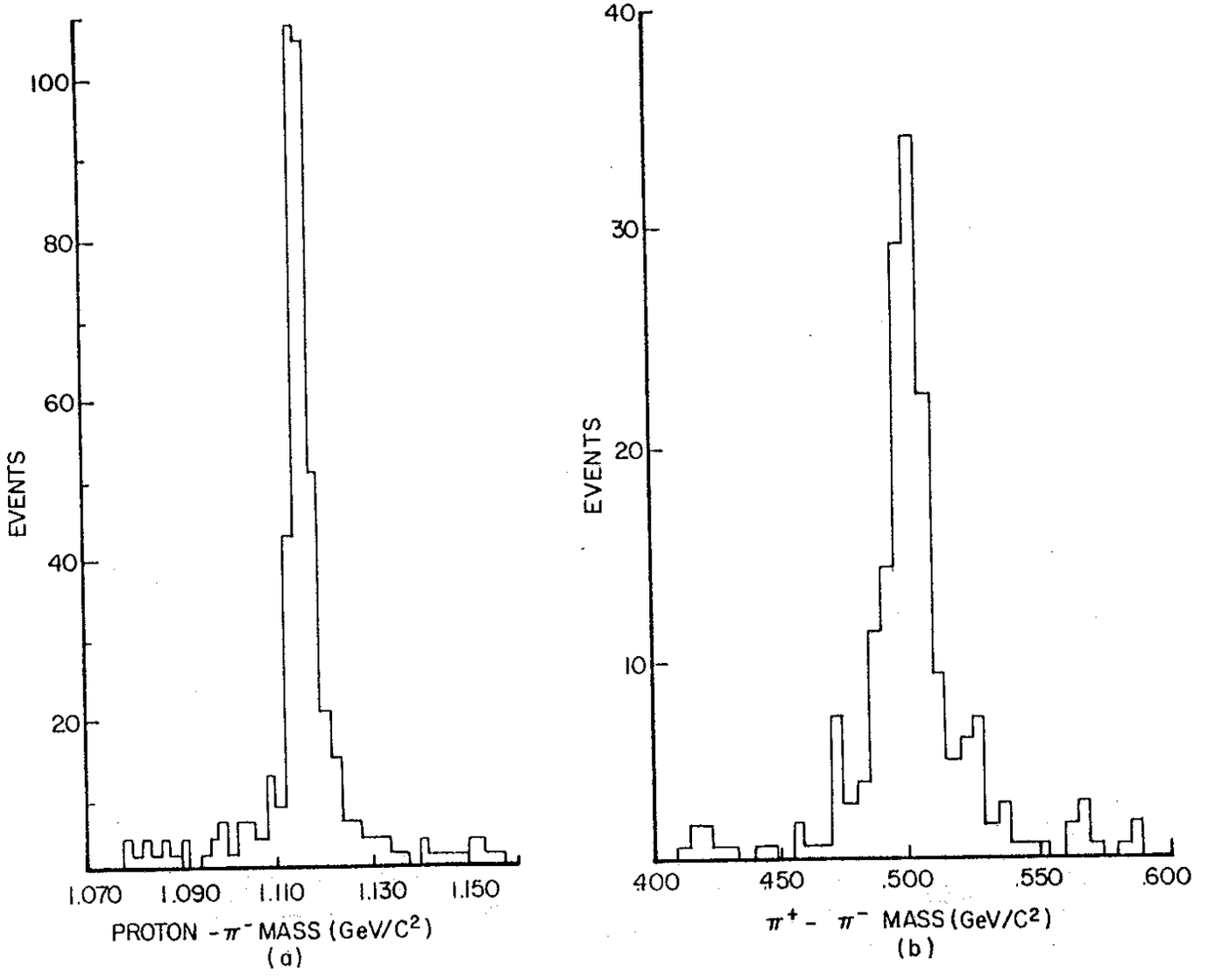

Fig. 17

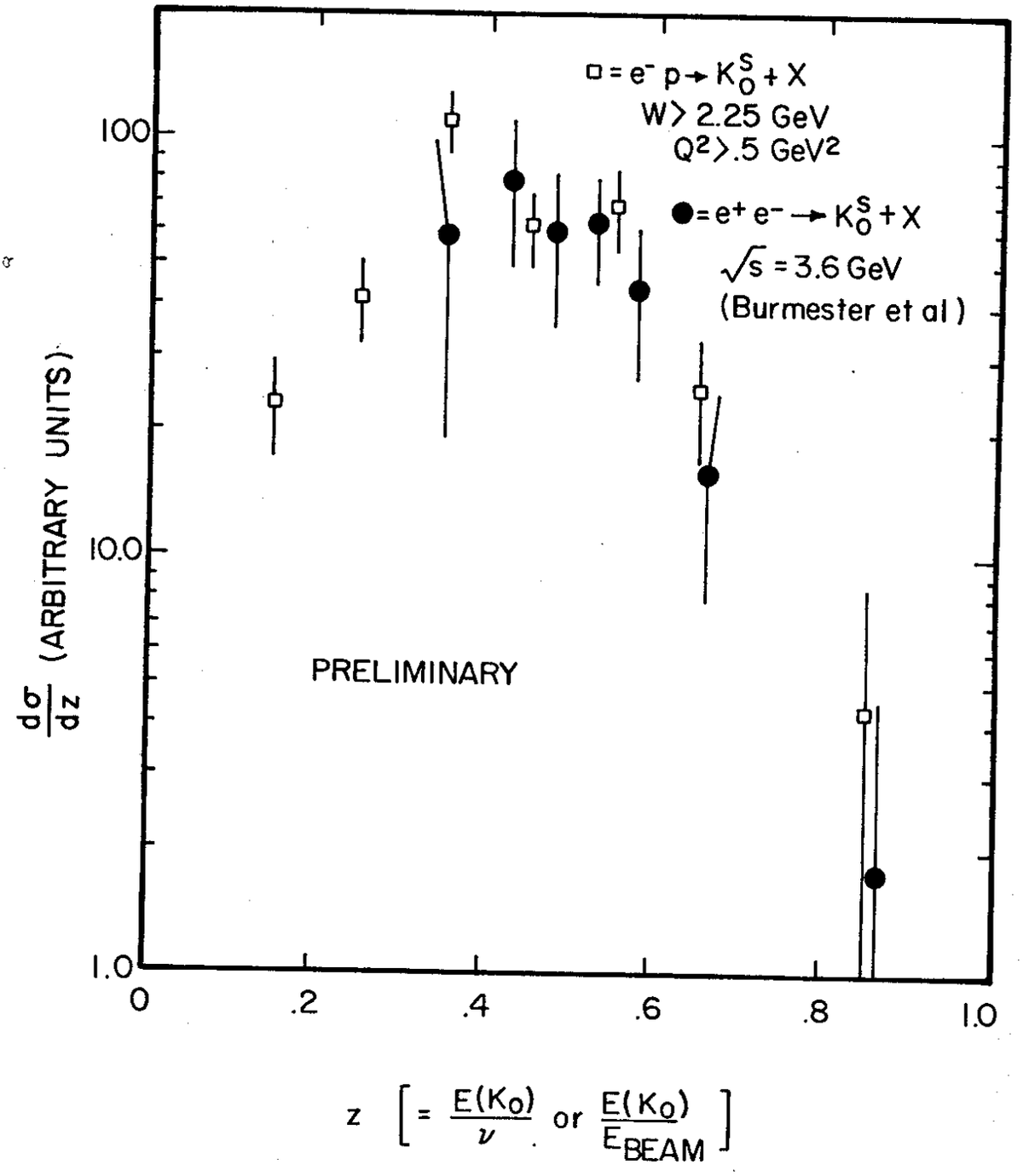
□ = e⁻ p → K⁰S + X
W > 2.25 GeV
Q² > .5 GeV²
● = e⁺ e⁻ → K⁰S + X
√s = 3.6 GeV
(Burmester et al)
PRELIMINARY
dσ/dz (ARBITRARY UNITS)
100
10.0
1.0
0
.2
.4
.6
.8
1.0
z [= E(K₀)/ν or E(K₀)/E_BEAM]

Fig. 18

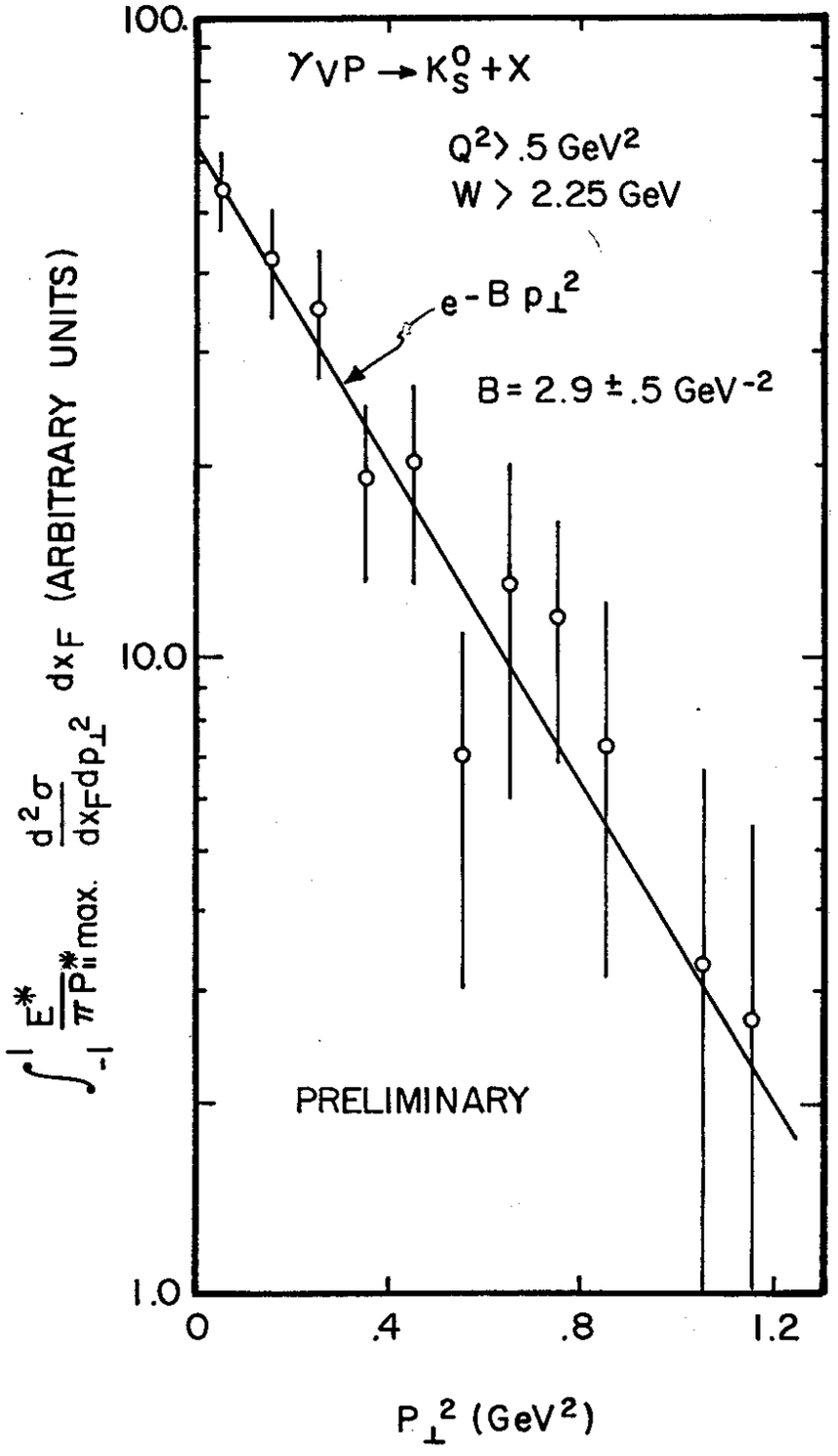
100.
10.0
1.0
0
.4
.8
1.2
$\gamma_{VP} \rightarrow K_S^0 + X$
$Q^2 > .5$ GeV^2
$W > 2.25$ GeV
$e - B\, p_\perp^2$
$B = 2.9 \pm .5$ GeV^{-2}
PRELIMINARY
$\int_{-1}^{1} \frac{E^*}{\pi P_{\parallel max}^*} \frac{d^2\sigma}{dx_F dp_\perp^2} dx_F$ (ARBITRARY UNITS)
$P_\perp^2$ (GeV^2)

Fig. 19

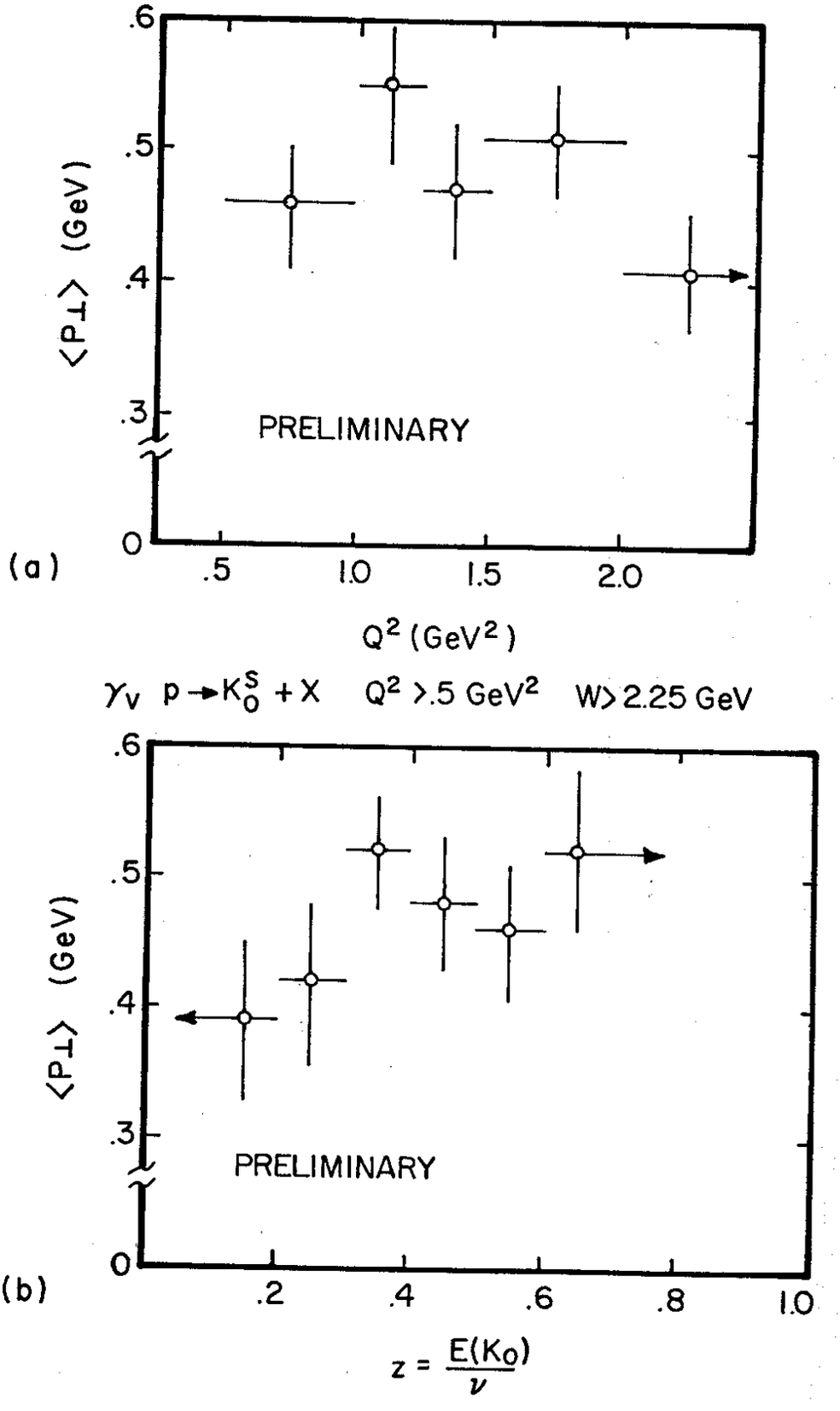
.6
.5
.4
.3
0
<P⊥> (GeV)
PRELIMINARY
(a)
.5
1.0
1.5
2.0
Q² (GeV²)
γV p → K⁰S + X Q² > .5 GeV² W > 2.25 GeV
.6
.5
.4
.3
0
<P⊥> (GeV)
PRELIMINARY
(b)
.2
.4
.6
.8
1.0
z = E(K0) / ν

Fig. 20

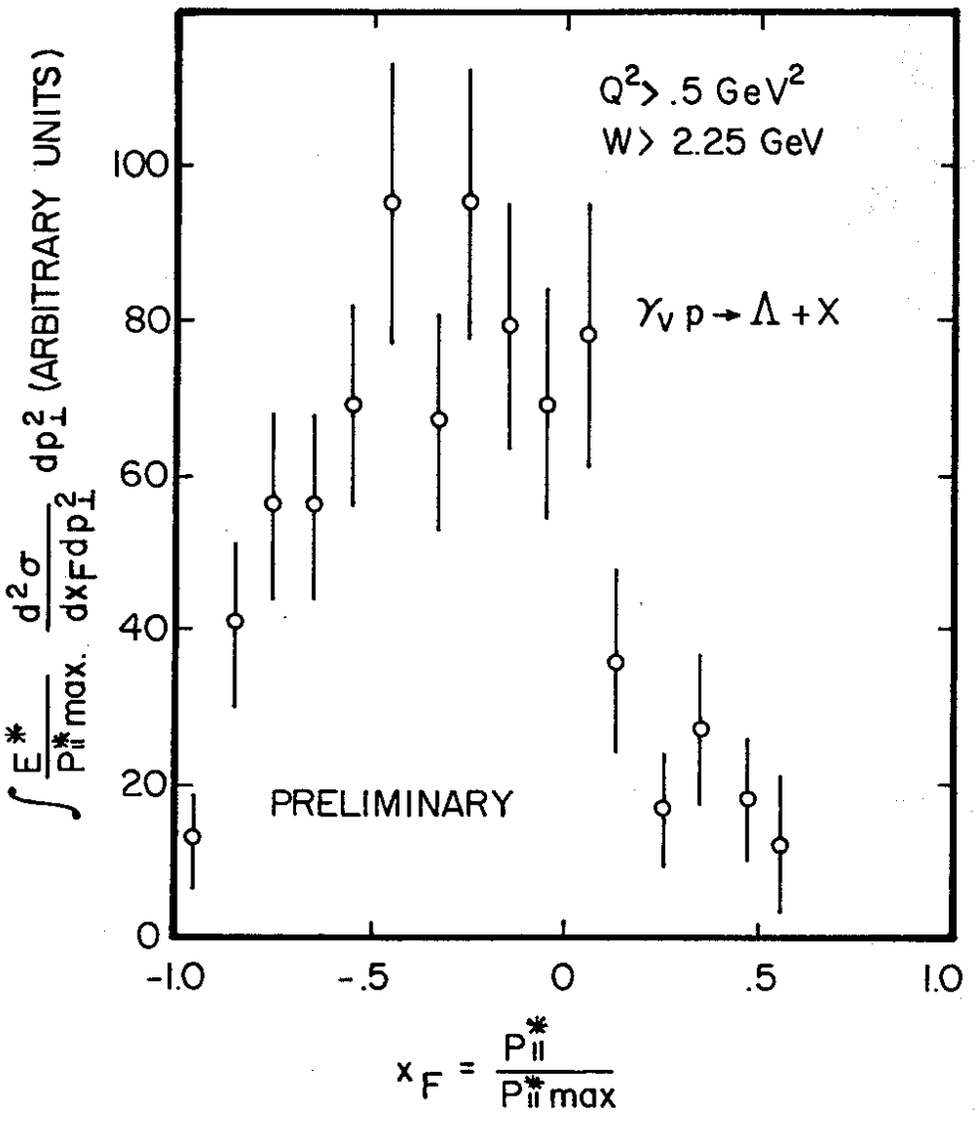
$Q^2 > .5$ GeV^2
$W > 2.25$ GeV
$\gamma_V p \to \Lambda + X$
PRELIMINARY
$\int \frac{E^*}{P^*_{\parallel max.}} \frac{d^2\sigma}{dx_F dp_\perp^2} dp_\perp^2$ (ARBITRARY UNITS)
$x_F = \frac{P^*_\parallel}{P^*_{\parallel max}}$
0
20
40
60
80
100
-1.0
-.5
0
.5
1.0

Fig. 21

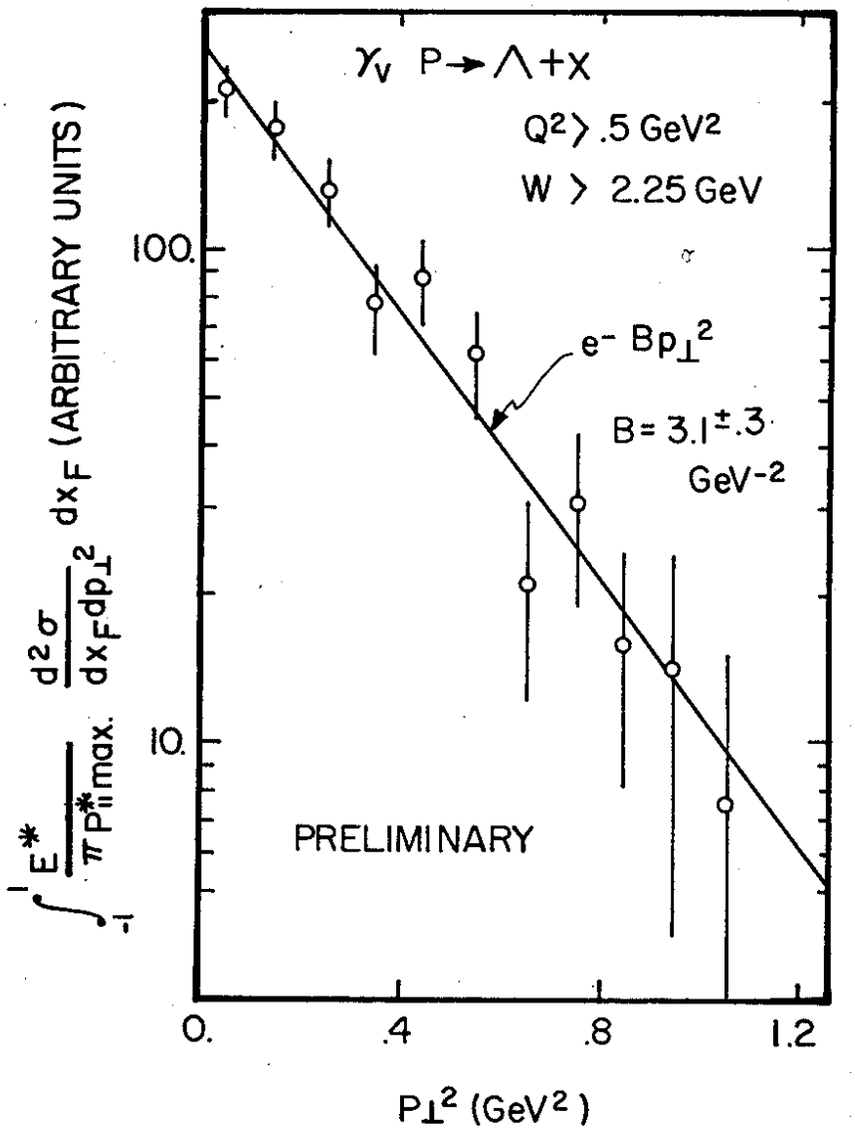
γ_V P → Λ + X
Q² > .5 GeV²
W > 2.25 GeV
e⁻ Bp⊥²
B = 3.1 ± .3 GeV⁻²
PRELIMINARY
100.
10.
0.
.4
.8
1.2
P⊥² (GeV²)
$\int_{-1}^{1} \frac{E^*}{\pi P^*_{\parallel max.}} \frac{d^2\sigma}{dx_F dp_\perp^2} dx_F$ (ARBITRARY UNITS)

Fig. 22

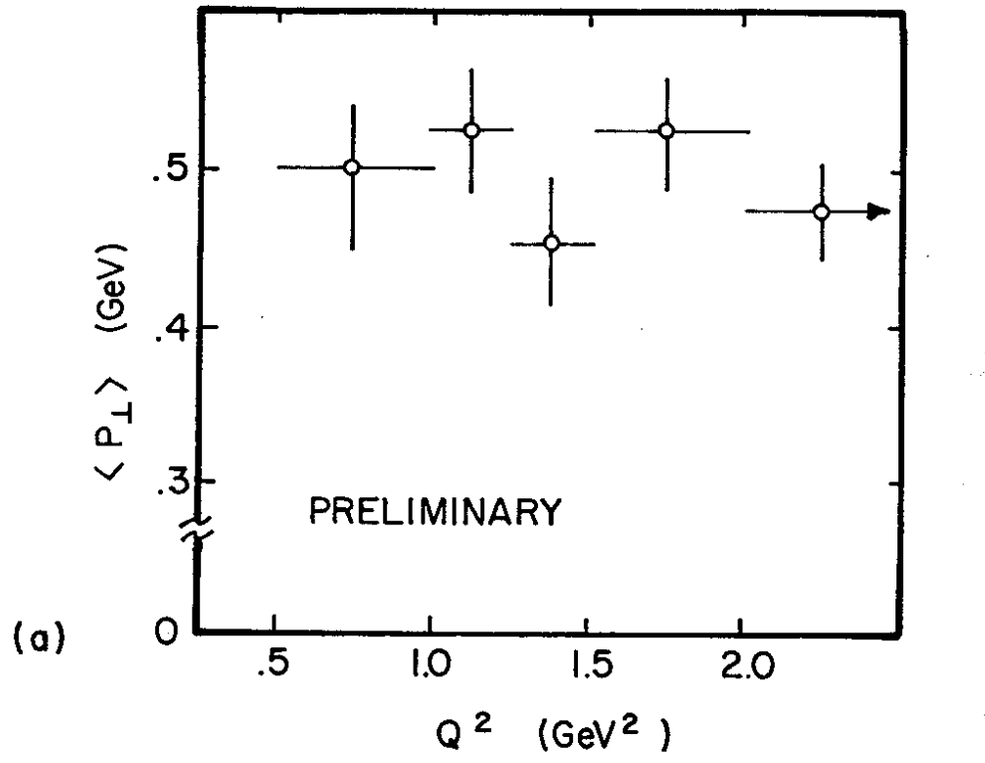

$\gamma_v p \to \Lambda + X$ $Q^2 > .5$ GeV^2 $W > 2.25$ GeV

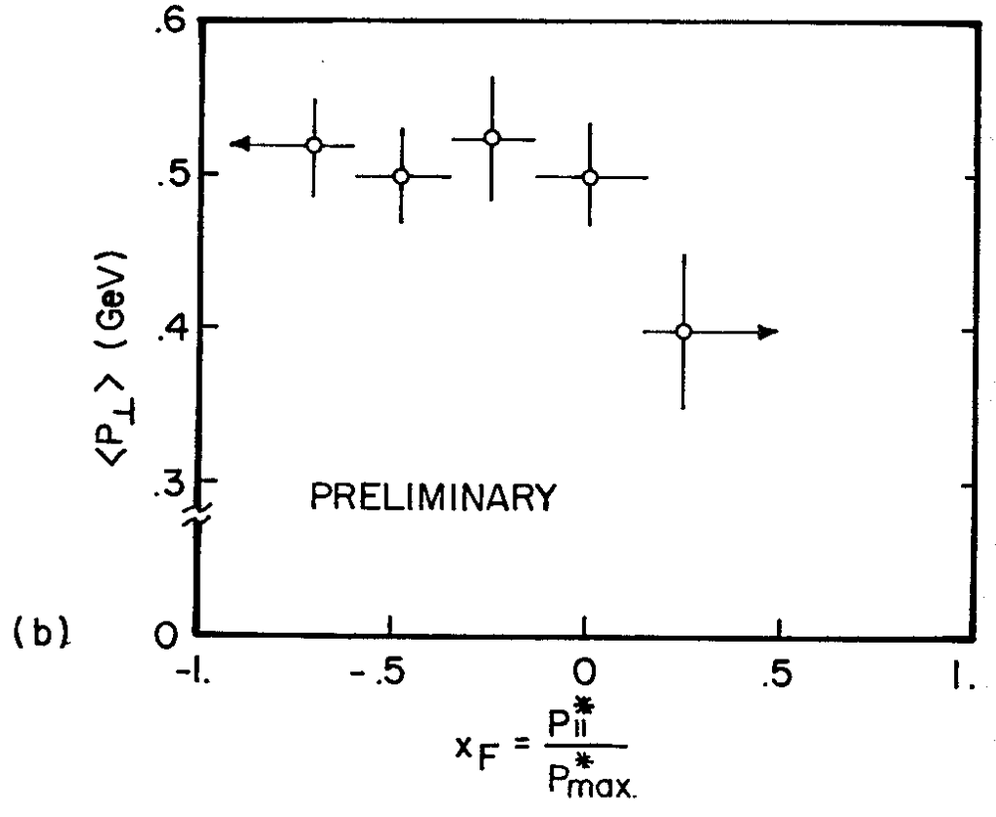

Fig. 23

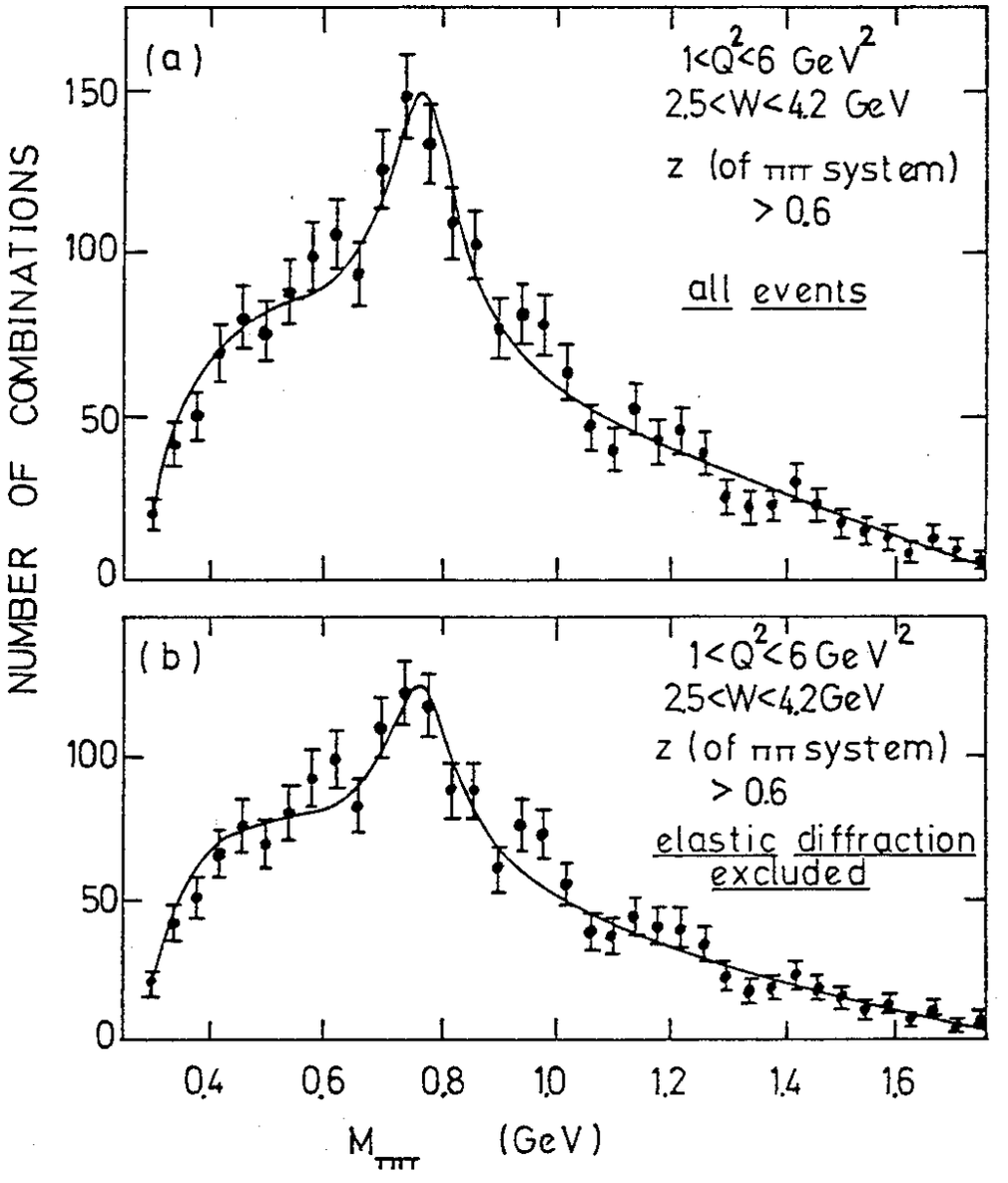
(a)
1<Q²<6 GeV²
2.5<W<4.2 GeV
z (of ππ system)
> 0.6
all events
(b)
1<Q²<6 GeV²
2.5<W<4.2GeV
z (of ππ system)
> 0.6
elastic diffraction
excluded
NUMBER OF COMBINATIONS
150
100
50
0
0.4
0.6
0.8
1.0
1.2
1.4
1.6
M_ππ (GeV)

Fig. 24

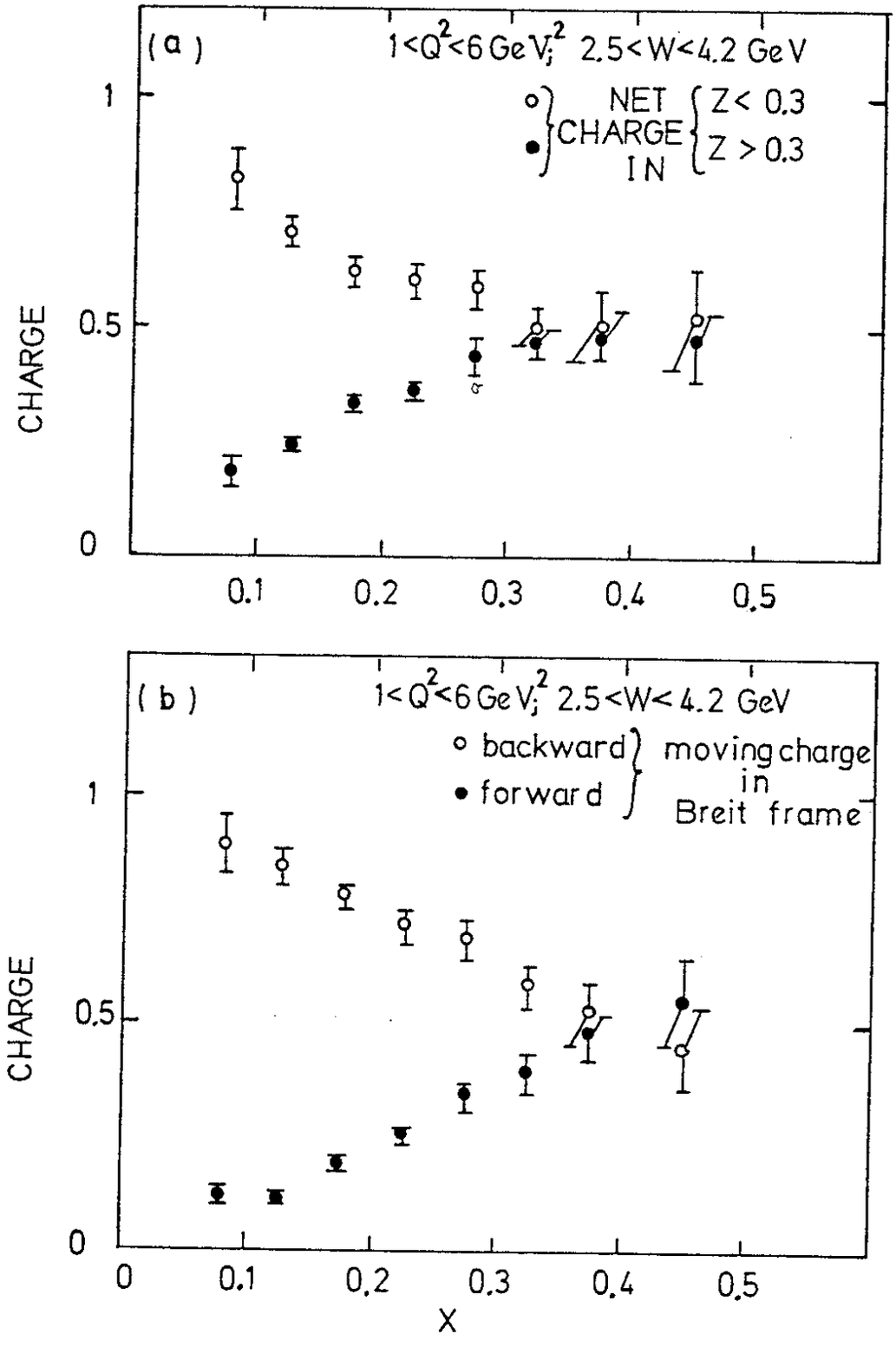
(a)
1<Q²<6 GeV² 2.5<W<4.2 GeV
NET CHARGE IN
Z< 0.3
Z > 0.3
CHARGE
1
0.5
0
0.1
0.2
0.3
0.4
0.5
(b)
1<Q²<6 GeV² 2.5<W<4.2 GeV
backward
forward
moving charge in Breit frame
CHARGE
1
0.5
0
0
0.1
0.2
0.3
0.4
0.5
X

Fig. 25